Global Biogeochemical Cycles

RESEARCH ARTICLE
10.1029/2024GB008202

The Changing Biological Carbon Pump of the South Atlantic Ocean

L. Delaigue[1], O. Sulpis[2,3], G.-J. Reichart[1,3], and M. P. Humphreys[1]

[1]Department of Ocean Systems (OCS), NIOZ Royal Netherlands Institute for Sea Research, Den Burg, The Netherlands, [2]CEREGE, Aix Marseille University, CNRS, IRD, INRAE, Collège de France, Aix-en-Provence, France, [3]Department of Earth Sciences, Utrecht University, Utrecht, The Netherlands

Key Points:

- The South Subtropical Convergence (SSTC) at 40°S in the Atlantic Ocean shows an intensified biological carbon pump, amidst uncertainties
- Discrepancies in trends between oxygen utilization and nitrate concentrations provide two distinct estimates of the biological carbon pump
- Local and far-field processes affect remineralization at 40°S, but their relative contributions cannot yet be precisely quantified

Supporting Information:

Supporting Information may be found in the online version of this article.

Correspondence to:

L. Delaigue and M. P. Humphreys, louise.delaigue@nioz.nl; matthew.humphreys@nioz.nl

Citation:

Delaigue, L., Sulpis, O., Reichart, G.-J., & Humphreys, M. P. (2024). The changing biological carbon pump of the South Atlantic Ocean. *Global Biogeochemical Cycles*, *38*, e2024GB008202. https://doi.org/10.1029/2024GB008202

Received 11 APR 2024
Accepted 25 AUG 2024

Author Contributions:

Conceptualization: L. Delaigue, M. P. Humphreys
Data curation: L. Delaigue, M. P. Humphreys
Investigation: L. Delaigue, O. Sulpis, M. P. Humphreys
Methodology: L. Delaigue
Software: L. Delaigue
Visualization: L. Delaigue
Writing – original draft: L. Delaigue
Writing – review & editing: L. Delaigue, O. Sulpis, G.-J. Reichart, M. P. Humphreys

Abstract Global marine anthropogenic CO_2 inventories have traditionally emphasized the North Atlantic's role in the carbon cycle, while Southern hemisphere processes are less understood. The South Subtropical Convergence (SSTC) in the South Atlantic, a juncture of distinct nutrient-rich waters, offers a valuable study area for discerning the potential impacts of climate change on the ocean's biological carbon pump (C_{soft}). Using discrete observations from GLODAPv2.2022 and BGC-Argo at 40°S in the Atlantic Ocean from 1972 to 2023, an increase in dissolved inorganic carbon (DIC) of $+1.44 \pm 0.11$ µmol kg^{-1} yr^{-1} in surface waters was observed. While anthropogenic CO_2 played a role, variations in the contribution of C_{soft} were observed. Discrepancies emerged in assessing C_{soft} based on the tracers employed: when using AOU, $C_{soft(AOU)}$ recorded an increase of $+0.20 \pm 0.03$ µmol kg^{-1} yr^{-1}, while using nitrate as the reference, $C_{soft(NO3)}$ displayed an increase of $+0.85 \pm 0.07$ µmol kg^{-1} yr^{-1}. Key processes such as water mass composition shifts, changes in oxygenation, remineralization in the Southern Ocean, and the challenges they pose in accurately representing the evolving C_{soft} are discussed. These findings highlight that while global studies primarily attribute DIC increase to anthropogenic CO_2, observations at 40°S reveal an intensified biological carbon pump, showing that regional DIC changes are more complex than previously thought and emphasizing the need for better parameterizations to compute the BCP in the marine carbon budget.

Plain Language Summary The South Atlantic Ocean at 40°S has experienced changes in dissolved inorganic carbon (DIC) over the years, affecting its carbon composition. This study running from 1972 to 2023 showcased an increase in the DIC down to 2,000 m deep. While anthropogenic CO_2 has traditionally been seen as the major contributor, the biological carbon pump's activity, influenced by various ocean processes, emerged as a significant driver. Specifically, factors such as photosynthesis, organic matter remineralization, sea ice movements, and freshwater influx from melting ice play pivotal roles in dictating oxygen and nitrate levels, both crucial components to predict the biological carbon pump's contribution to DIC. Our findings emphasize that this enhanced biological pump might contribute as much as human-made CO_2 to DIC in certain ocean regions. If unchecked, these changes could recalibrate ocean carbon budgets and predictions with potential shifts in water mass compositions, demanding more vigilant future monitoring.

1. Introduction

The ocean has been acting as a sink for anthropogenic CO_2, absorbing an estimated 24% of anthropogenic CO_2 since the beginning of the industrial era, thus significantly mitigating climate change (Friedlingstein et al., 2023; Gruber et al., 2023). Part of this anthropogenic carbon remains in the form of dissolved inorganic carbon (DIC) and is transported into the ocean interior (Davila et al., 2022; Gruber et al., 2019; Khatiwala et al., 2009; Sabine & Tanhua, 2010; Sarmiento et al., 1992), and part of it is incorporated by marine organisms into organic matter or calcium carbonate (Heinze et al., 1991; Sarmiento et al., 1998; Volk & Hoffert, 1985).

The sequence of processes that store atmospheric carbon as biogenic matter at the surface ocean and sequester a small fraction of it in deep-sea sediments, where it can be stored permanently, is named the "biological pump" (Riebesell et al., 2009). While recent studies have focused on quantifying anthropogenic CO_2 uptake by the ocean at the air-sea interface, or its fate into the ocean interior as DIC, little is known about its effect on the removal by the biological carbon pump (BCP) over recent years, despite its importance for understanding future ocean carbon cycling. Biological processes in the upper ocean annually convert approximately 50–60 gigatons of dissolved inorganic carbon into organic matter (De La Rocha & Passow, 2014). Out of this amount, around 10% is

transported out of the surface ocean in the form of organic carbon (De La Rocha & Passow, 2014). Through this natural and anthropogenic carbon export, the BCP lowers atmospheric CO_2 levels by ∼200 ppm relative to a world without it (Parekh et al., 2006; R. G. Williams & Follows, 2011). It is thus essential that we understand the drivers and variability of the BCP and its vulnerability to current anthropogenic changes to predict future climate. However, the complexity of ecosystem functioning and composition makes estimates of both present-day and future organic carbon exports poorly constrained in models and observations (Henson et al., 2012, 2022; Laufkötter et al., 2016; Marsay et al., 2015).

The oceanic distribution of DIC is mainly controlled by three pumps: the biological processes of photosynthesis and remineralization (i.e., the soft-tissue pump, C_{soft}), the formation and dissolution of calcium carbonate (i.e., the carbonate pump, C_{carb}) and the uptake of natural and anthropogenic CO_2 (i.e., the solubility pump, C_{anth}; Gruber et al., 1996; Volk & Hoffert, 1985). While the solubility pump accounts for 30%–40% of ocean carbon export flux to the deep ocean (Gruber et al., 2002; Toggweiler et al., 2003), the remaining portion is transported from the sunlit surface to the deep ocean as photosynthetically fixed organic carbon by the soft tissue pump (Riebesell et al., 2009; Schlunegger et al., 2019). To quantify the rate of soft tissue and carbonate pump changes, one could monitor particulate organic and inorganic carbon sinking fluxes through time, but sediment trap data are sparse and associated with large uncertainties (Buesseler et al., 2007). Monitoring changes in DIC is also complicated because C_{soft}, C_{carb}, and C_{anth} cannot be readily distinguished from the DIC analyses themselves. Instead, one can unravel the different components of the carbon pump and changes therein by combining multiple proxies, such as the apparent oxygen utilization (AOU; the difference between the saturation oxygen concentration, $[O_{2,sat}]$ and the observed oxygen concentration, $[O_2]$), or release rates of organic-matter degradation byproducts, that is, NO_3^-, PO_4^{3-} or alkalinity. For the carbonate pump, calcification and dissolution can be tracked in seawater by measuring dissolved calcium or alkalinity changes (C.-T. A. Chen, 1978; Feely et al., 2004). Carbon sequestration by the soft tissue pump can be estimated from nutrient and oxygen observations, taking advantage of the constant stoichiometric ratios of carbon, nutrients, and oxygen in marine organic matter in the open ocean, also known as the Redfield Ratio (Ito & Follows, 2005; Redfield, 1958). Using the latter, these variables are converted back to carbon units in the natural components of DIC (C_{carb}, and C_{soft}) as well as anthropogenic CO_2 (C_{anth}), allowing for the disentanglement of changes in each DIC component.

Although global evaluations of the oceanic CO_2 inventory have often highlighted the North Atlantic Ocean as the primary region of interest for anthropogenic CO_2 subduction, with a storage estimated at 23% of global ocean anthropogenic CO_2 (Khatiwala et al., 2013; Sabine et al., 2004), the importance of southern hemisphere processes, such as the formation of Antarctic Intermediate Water (AAIW), has recently gained attention (Groeskamp et al., 2016; Landschützer et al., 2015). The South Subtropical Convergence (SSTC), an intersection point of low-macronutrient subtropical gyre waters and high-macronutrient Antarctic Circumpolar Current waters, is a significant biogeochemical feature of the South Atlantic Ocean (Browning et al., 2014). This convergence zone results in strong downwelling and pronounced surface gradients in salinity and temperature, leading to distinct water column stratification with shallow mixing in a thermally homogeneous surface layer, increasing light availability and productivity (Browning et al., 2014). Such stratification can impact the marine carbon cycle by potentially inhibiting the transport of heat, oxygen, and carbon dioxide deeper into the ocean (Li et al., 2020).

Simultaneously, the Southern Ocean is known for its high macronutrient supply, primarily from the upwelling of nutrient-rich deep waters (Moore et al., 2001; Tagliabue et al., 2014). These waters provide nitrate that fuels primary production. As organic matter produced in the Southern Ocean sinks to the SSTC region, it undergoes remineralization, converting back into inorganic nutrients. Nitrate concentrations can thus indicate the extent of remineralization in an area (Moore et al., 2001; Tagliabue et al., 2014), with higher concentrations suggesting that more organic matter has been remineralized. This enhanced remineralization, fueled by the increased nitrate supply from the Southern Ocean waters, may then contribute to a stronger soft tissue pump and carbon export to deeper waters (Boyd & Trull, 2007; Sarmiento, 2006). However, it is important to note that the Southern Ocean is a High Nutrient, Low Chlorophyll (HNLC) area, meaning that despite the abundance of macronutrients, primary productivity is often limited by the availability of micronutrients such as iron (Boyd & Trull, 2007). Behrenfeld et al. (2006) have shown a decrease in net primary productivity (NPP) with global warming in major parts of the Southern Ocean. This indicates that primary productivity is not uniformly enhanced and is influenced by factors such as nutrient availability and climate change impacts.

Although not historically prominent, anticipated changes in the BCP are emerging due to specific climatic and oceanographic drivers. Behrenfeld et al. (2006) reported alterations in ocean productivity linked to climate change, with increased stratification in some regions affecting primary production. Polovina et al. (2008) identified the expansion of subtropical gyres and associated shifts in phytoplankton communities in the Pacific. Furthermore, Orr et al. (2005) demonstrated that escalating CO_2 concentrations lead to ocean acidification, challenging marine calcifying organisms crucial for carbon sequestration. Considering these documented changes in diverse oceanic regions and the critical nature of the SSTC around 40°S in the Atlantic Ocean, it is plausible that similar dynamics will impact the BCP in this region.

In this study, we aim to quantify changes in the biological carbon pump at 40°S in the Atlantic Ocean. We leverage data from the GEOTRACES 40°S cruise, the first zonal expedition at this latitude in the South Atlantic to measure DIC. We join up all the other GLODAPv2.2022 cruises going perpendicularly and recent autonomous marine observations from the BGC-Argo array into a single analysis. This time series of marine carbonate chemistry measurements is used to calculate the rates of change in key variables and used to disentangle changes in the natural components of DIC (soft tissue pump, C_{soft} and carbonate pump, C_{carb}) from anthropogenic CO_2 (C_{anth}). We examine the underlying reasons for the divergence in BCP estimations, probing into the shifts in water mass composition within formation areas and delving into the effects of diminished oxygenation and heightened remineralization in the Southern Ocean. BCP estimates are then aligned with global carbon budgets, revealing potential gaps in our understanding, particularly how regional changes in the biological carbon pump, driven by climate change, might feedback into these estimates.

2. Materials and Methods

2.1. Discrete Measurements From GLODAPv2.2022

Data from 11 cruises along latitude 40°S in the Atlantic Ocean were extracted from the Global Ocean Data Analysis Project version 2 (GLODAPv2.2022; Lauvset et al. (2022), Figure 1; see Table S1 in Supporting Information S1) and analyzed. From these, only the GEOTRACES 40°S cruise occupied the entire latitudinal transect (Expocode #740H20111224, 2011, RRS James Cook; cruise #4095 in GLODAPv2.2022), while the rest either covered it partially or crossed it latitudinally. Only stations with a bottom depth beyond 1,000 m were considered as to remove data falling on the continental shelf and/or slope. Rather than using original cruise data, the analysis benefited from the GLODAPv2.2022 applied adjustment of properties, making the analysis internally consistent. Hydrographic parameters included temperature (T), practical salinity (S_P), dissolved oxygen ($[O_2]$), dissolved inorganic carbon (DIC), total alkalinity (A_T) and nitrate (NO_3^-). Only data with a quality control deemed "Good" (Flag = 2) were used. This analysis considered the full depth of the water column, with an emphasis on the central and intermediate waters during the discussion as most change has been observed in these waters (Piñango et al., 2022).

2.2. Autonomous Data From BGC-Argo Floats

Float data were downloaded from the Argo Global Data Assembly Center (AOML) for an 8-year period (2015–2023). Only months matching GLODAPv2.2022 were kept (i.e., October, November, December, January, February, and March). Selected floats all fell within a defined geographical area matching GLODAPv2.2022 (38°S–42°S, 15°W–50°E, Figure 1). All selected float profiles included temperature (T), practical salinity (S_P), dissolved oxygen ($[O_2]$), pH on the total scale (pH_T) and nitrate (NO_3^-) (i.e., 9 floats, 73 profiles; see Table S2 in Supporting Information S1). All BGC-Argo profiles used here were downloaded as Delayed Mode files, which are designed for scientific exploitation and represent the highest quality of data to possibly extract climate-related trends (Bittig et al., 2019). Only adjusted data that were flagged as "Good" (QC = 1) were used in this study, except for T and S_P, for which estimated values (QC = 8) were used when adjusted data was missing. Each float profile was treated as the equivalent of a GLODAPv2.2022 cruise in the analysis.

2.3. Derived Variables

For all BGC-Argo profiles, A_T was calculated using Python SciPy nonlinear least-square fitting (v.1.9.3; Virtanen et al., 2020) with T, S_P and depth as input parameters. More information can be found in Supporting Information S1, along with a comparison to Lee et al. (2006) A_T estimates (Text S1 and Figures S1–S3 in Supporting Information S1).

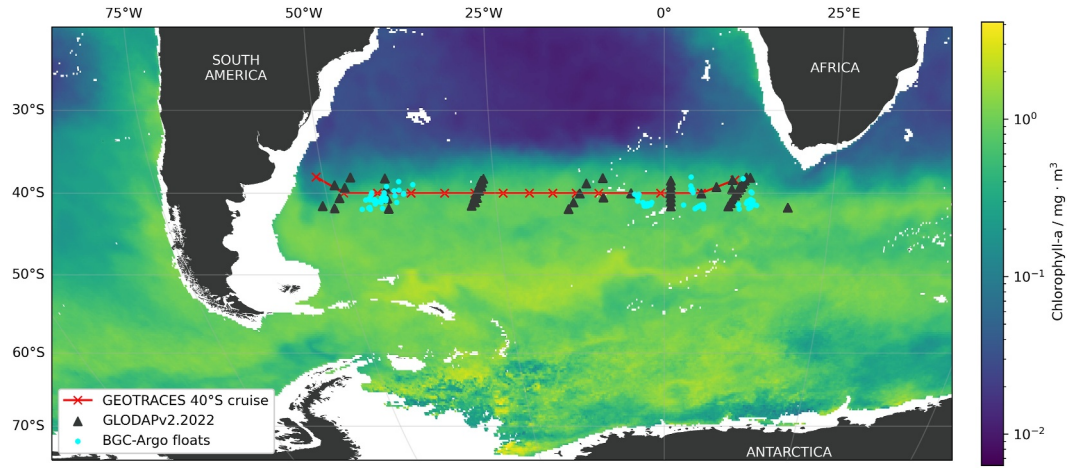

Figure 1. Map of the study region in the South Atlantic Ocean. Red lines with crosses show the trajectory of the longitudinal GEOTRACES 40°S cruise. Black triangles show the location of GLODAPv2.2022 cruises. Turquoise blue dots show the BGC-Argo float data. Color scale of the background map shows chlorophyll-a concentration (log-scale; Chl-a data downloaded from CMEMS following Sauzède et al., 2016).

Neutral density surfaces (γ^n) were calculated from T, S_P, pressure, latitude and longitude using the EOS-80 Legacy toolbox for MATLAB® (MathWorks®, USA). Absolute salinity (S_A) and potential temperature (θ) were calculated from T, S_P, and pressure using the Gibbs-SeaWater Oceanographic Toolbox for MATLAB® (MathWorks®, USA). Apparent oxygen utilization (AOU) was calculated from θ, S_A and [O_2] using the combined fit coefficients from Garcia and Gordon (1992). These calculations were carried out for all data sets without the above variables either already measured or calculated. The Mixed Layer Depth (MLD) for each station during the GEOTRACES 40°S cruise was determined using a density criterion, with density calculated from T, S_P, and pressure data according to the Python implementation of the Gibbs SeaWater (GSW) Oceanographic Toolbox of TEOS-10 (v. 3.6.16; McDougall & Barker, 2011). The MLD was defined as the depth at which the water's density increases by 0.03 kg m^{-3} compared to the surface. Then, the mean MLD and mean neutral density across all stations for that cruise were calculated, resulting in an average MLD of 54m ($\gamma^n \approx 25.8$). We performed this calculation to distinguish the upper layer from the rest of the water column, which is essential for separating deeper water biogeochemical processes which fundamentally differ from those in the surface layer. Our results specifically focus on the waters below the MLD.

2.4. Marine Carbonate System Parameters

Depending on available variables, remaining marine carbonate parameters were calculated from any pair of DIC, A_T, pH_T using PyCO2SYS v1.8.1 (Humphreys et al., 2022), and with the carbonic acid dissociation constants from Sulpis et al. (2020), bisulfate dissociation constant from Dickson (1990), the total boron:chlorinity from Uppström (1974) and the hydrogen fluoride dissociation constant from Dickson and Riley (1979). When available for GLODAPv2.2022, phosphate and silicate were included in the carbonate system calculations but their inclusion did not affect the results significantly as their concentrations are relatively low in the open ocean (mean difference of −0.007 for pH and 1.51% for pCO_2). Calculated parameters include pH on the total scale (pH_T) and the seawater partial pressure of CO_2 (pCO_2) for GLODAPv2.2022 data, and DIC and pCO_2 for BGC-Argo data.

2.5. Interpolations

For each year, all variable data were clustered and interpolated vertically to γ^n levels using Piecewise Cubic Hermite Interpolating Polynomial (PCHIP) fits to observations (Figure 2; Fritsch & Carlson, 1980; Humphreys et al., 2016). Briefly, the PCHIP method uses monotonic cubic splines to find the value of new points. This allows for comparability between all cruises across the transect as averaging on isopycnals mimics real oceanic mixing processes occurring primarily along isopycnals, or, more precisely, along neutral density surfaces. Data were not extrapolated beyond the measured observational γ^n levels.

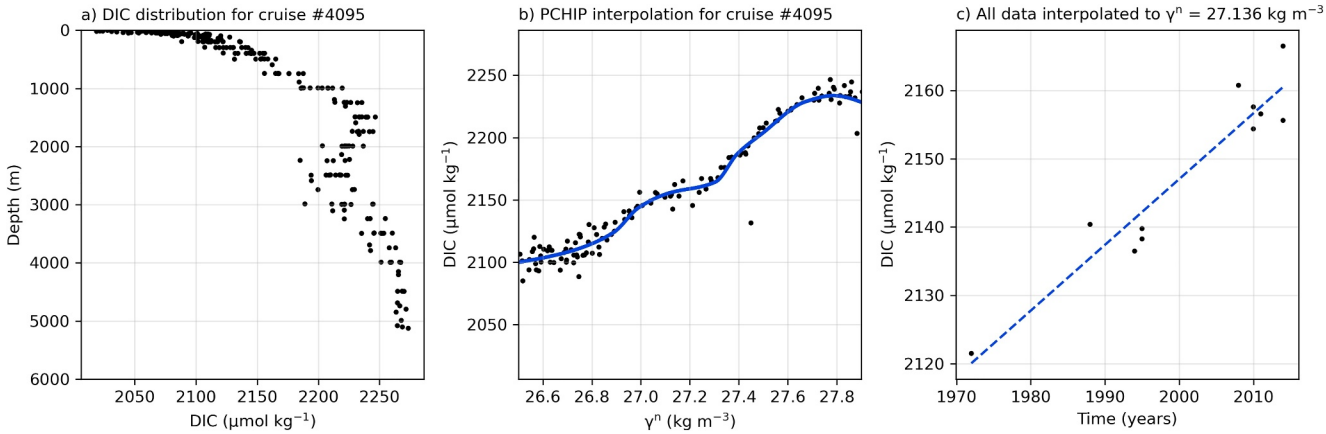

Figure 2. Analysis routine for each cruise and float profile, here showing for GEOTRACES 40°S longitudinal cruise: (a) the vertical distribution of DIC; (b) the PCHIP interpolation for DIC along neutral density levels; and (c) the linear regression at a given neutral density level.

2.6. Rates of Change

For each variable, ordinary least square regressions were used to determine their rate of change at each γ^n level (Figure 2). All rates of change are reported as $\frac{dX}{dt} \pm \boldsymbol{U}$, where $\boldsymbol{X}$ is the variable and $\boldsymbol{U}$ is the associated uncertainty. Regressions were achieved using the Python library SciPy v.1.9.3 (Virtanen et al., 2020). All rates of change were calculated with the same time range for all variables, that is, from 1972 to 2023, except for silicate and phosphate for which only GLODAPv2.2022 data are available up to 2014.

2.7. CO_2 Components

Three pumps contribute to the distribution of DIC: photosynthesis and remineralization (C_{soft}), the formation and dissolution of calcium carbonate (C_{carb}), and uptake of natural and anthropogenic CO_2 (C_{anth}; Gruber et al., 1996; Volk & Hoffert, 1985). Thus, DIC changes can be described as

$$\Delta T_{DIC} = \Delta C_{soft} + \Delta C_{carb} + \Delta C_{anth}. \quad (1)$$

Biological activity converts dissolved inorganic nutrients to particulate organic matter, which is transported down the water column through gravitational settling and active transport by marine organisms. During their settling in deeper waters, carbon and nutrients are returned to their dissolved inorganic forms through remineralization while taking up O_2 and thus increasing AOU (Redfield, 1963). This process drives the soft tissue pump, which is defined as

$$\Delta C_{soft(AOU)} = -R_{C/O_2} \cdot \Delta AOU, \quad (2a)$$

$$\Delta C_{soft(NO3)} = R_{C/NO_3^-} \cdot \Delta NO_3^-, \quad (2b)$$

where $\boldsymbol{R}_{C/X}$ is the increase in $\boldsymbol{C}$ as a fraction of X variable consumption during remineralization. Changes in nitrate (ΔNO_3^-) which, like changes in AOU (ΔAOU), reflect biological processes as well as physical mixing in the ocean. Specifically, ΔNO_3^- indicates the net effect of nitrate consumption during phytoplankton growth and release during remineralization. Thus, Equations 2a and 2b assume that changes occur under conditions influenced by both preformed properties—those characteristics established at the surface before subduction—and isopycnal mixing, which refers to mixing along surfaces of equal density.

In this study, we used the ratio from Anderson and Sarmiento (1994) as follows:

$$\begin{aligned} &P\text{:}\ N\text{:}\ C\text{:}\ -O_2 \\ &1\text{:}\ 16\text{:}\ 117\text{:}\ 170, \end{aligned} \quad (3)$$

Thus, R_{C/O_2} and R_{C/NO_3^-} can be assumed to be a constant value of -0.688 ± 0.092 and 7.31 ± 0.092 respectively (Anderson & Sarmiento, 1994).

The formation and dissolution of $CaCO_3$ makes up the carbonate pump, where an increase in $\boldsymbol{C}$ is coupled with a two-fold increase in A_T (Wolf-Gladrow et al., 2007):

$$\Delta C_{\text{carb}} = 0.5 \cdot (\Delta A_T - R_{N/O_2} \cdot \Delta \text{AOU}), \tag{4}$$

where R_{N/O_2} is a ratio of -0.0941 ± 0.0081 (Anderson & Sarmiento, 1994).

The remaining term, namely the solubility pump, relies on the uptake of anthropogenic CO_2 (ΔC_{anth}) and the CO_2 air-sea disequilibrium (ΔC_{diseq}) at the time the water lost contact with the atmosphere (Gruber et al., 1996). Assuming $\Delta C_{\text{diseq}} = 0$, that is, no significant long-term trend in air-sea CO_2 disequilibrium, the accumulated anthropogenic ΔC_{anth} is defined as

$$\Delta C_{\text{anth}} = \Delta C_{\text{sol}} - \Delta C_{\text{diseq}} \approx \Delta C_{\text{sol}}. \tag{5}$$

where ΔC_{sol} represents the change in carbon content due to solubility processes, reflecting the amount of anthropogenic CO_2 absorbed by the ocean through physical and chemical processes. In this context, considering $\Delta C_{\text{diseq}} = 0$ is justified based on the assumption that the long-term trends in air-sea CO_2 disequilibrium do not significantly affect the solubility pump on the timescales we are examining. While short-term and regional variations in disequilibrium are acknowledged, the overall impact on long-term global carbon uptake is considered minimal for this analysis (Jones et al., 2014; Nowicki et al., 2024).

2.8. Determining the Transition Depth for C_{soft} Significance

To determine the neutral density level at which the difference between $C_{\text{soft(NO3)}}$ and $C_{\text{soft(AOU)}}$ stops being statistically significant, we conducted an analysis incorporating the individual errors of each estimate. For each neutral density level, the estimates of $C_{\text{soft(NO3)}}$ and $C_{\text{soft(AOU)}}$ were adjusted by their respective errors to generate additional sample values. Specifically, for each estimate, three values were considered: the estimate itself, the estimate plus its error, and the estimate minus its error. These samples were then used in a paired t-test to compare the distributions of $C_{\text{soft(NO3)}}$ and $C_{\text{soft(AOU)}}$ at each neutral density level.

The t-test was applied iteratively from the deepest depths toward shallower depths, testing for significant differences at each neutral density level using a significance level of 0.05. The analysis identified the neutral density level where the p-value first exceeded this threshold, indicating that the differences between $C_{\text{soft(NO3)}}$ and $C_{\text{soft(AOU)}}$ were no longer statistically significant.

2.9. Natural CO_2 Inventory Change

The study area considered here is bound by latitudes -40.5 to $-39.5°$ and longitude -50 to $15°$ for a total surface area of 616,300 km^2.

Changes in $C_{\text{soft(AOU)}}$ and $C_{\text{soft(NO3)}}$ were multiplied by a density factor of 1028 to convert units from $\mu mol\ kg^{-1}\ yr^{-1}$ to $\mu mol\ m^3\ yr^{-1}$. The resulting values were integrated along the water column by sum ($C_{\text{soft(AOU)-int}}$ and $C_{\text{soft(NO3)-int}}$). Assuming lateral homogeneity, $C_{\text{soft(AOU)-int}}$ and $C_{\text{soft(NO3)-int}}$ were further converted to GtC $m^2\ yr^{-1}$ and integrated over the surface of the study area.

2.10. Uncertainty Propagation

For GLODAPv2.2022, uncertainties were assigned based on Table 3 of Lauvset et al. (2022) for all data dated from after 1994 (i.e., first use of CRMs). For data prior to 1994, an uncertainty of $\pm 17.2\ \mu mol\ kg^{-1}$ was assigned (Dickson, 1992). Most BGC-Argo floats included the error for each adjusted variable. Some uncertainties were missing for T and S_P, for which values were assigned based on N. L. Williams et al. (2017) and Mignot et al. (2019), except for the calculated A_T for which the fit RMSE was used ($5.5\ \mu mol\ kg^{-1}$, see Text S1 in Supporting Information S1). Uncertainties for variables calculated using PyCO2SYS v1.8.1 were propagated using the independent uncertainty argument (Humphreys et al., 2022).

In the process of quantifying analysis uncertainty, a multifaceted approach was employed to ensure comprehensive error propagation. To assess the uncertainty in the rates of change, a differential analysis was undertaken, calculating the derivatives for all variables under consideration (i.e., forward-finite differences). Each variable was incrementally altered by adding or subtracting a value derived from its assigned uncertainty. This alteration was specific to the variable's nature, and the impact of these perturbations on the overall outcome was studied through a repeated linear regression on the data set, now modified to reflect these adjustments. The differences between the coefficients of the original and modified data sets provided insights into the sensitivity of each variable. After normalization, these differences gave the true derivatives. By juxtaposing these derivatives with known measurement uncertainties, a comprehensive error term for each variable's rate of change was determined, offering a robust assessment of propagated uncertainties. This step provided a foundational understanding of how minor perturbations in each variable could influence the outcome.

Subsequently, to further refine the understanding of the variability and potential uncertainties inherent in the data set, a bootstrapping technique was applied. Essentially, the data for specific cruises was selectively omitted in a series of simulations, creating a variety of modified data sets. This non-parametric statistical method facilitated the estimation of the distribution of sample statistics by resampling with replacement, thereby offering insights into the potential variability of the results.

Finally, for each measured variable, an internal bias was determined for each cruise or float profile using the standard deviation of each linear regression from the rates of change estimation. All uncertainties were then synthesized to produce a combined error estimate. This layered approach ensured a robust assessment of analysis uncertainty, capturing both the immediate sensitivities of the variables and the broader variability in the data set.

3. Results

Multi-decadal rates of change for all available and derived carbonate parameters were calculated using GLODAPv2.2022 and BGC-Argo data along latitude 40°S for the period 1972–2023. Changes in individual variables are reported in Figure 3, while the calculated change in each component of DIC is shown in Figure 4. For all variables, little to no change was observed deeper than ∼2,000 m in the water column; thus, only data down to this depth are presented here.

On average, surface waters became warmer and fresher, which was reflected in A_T with a slight negative change. Slight decreases of -0.04 ± 0.0006°C yr^{-1} in θ and -0.01 ± 0.0002 yr^{-1} in S_P were observed in the top ∼300 m ($\gamma^n < 27.0$ kg m^{-3}), with virtually no change deeper in the water column (Figures 3a and 3b). This was closely mirrored by A_T, which showed a maximum decrease of -0.49 ± 0.11 µmol kg^{-1} yr^{-1} within the top ∼200 m ($\gamma^n < 26.8$ kg m^{-3}), while showing no change deeper in the water column (Figure 3c).

Surface waters also showed signs of deoxygenation and increased AOU (Figure 3h), while the nitrate pool increased (Figure 3i). [O_2] decreased down to ∼900 m ($\gamma^n \approx 27.4$ kg m^{-3}) with a minimum $\Delta[O_2]$ of -0.56 ± 0.05 µmol kg^{-1} yr^{-1} (Figure 3g). Deeper than 150 m, the AOU increased by a maximum of $+0.54 \pm 0.02$ µmol · kg^{-1} · yr^{-1}, from the surface down to ∼2,000 m ($\gamma^n \approx 27.9$ kg m^{-3}; Figures 3h and 3i). Both AOU and [O_2] converged toward no change at around ∼300 m ($\gamma^n \approx 27.0$ kg m^{-3}) before continuing their respective decrease/increase. An important increase in NO_3^- was observed with a peak of $+0.14 \pm 0.01$ µmol · kg^{-1} · yr^{-1} for the first ∼150 m ($\gamma^n < 26.7$ kg m^{-3}), while slowly converging toward no change by ∼1,000 m ($\gamma^n \approx 27.5$ kg m^{-3}; Figure 3i).

For the analysis of the N/P ratio and [Si], the data is limited to measurements up to 2014. This limitation arises because the BGC-Argo floats are not equipped to measure phosphate and silicate, thus only GLODAPv2.2022 data was used. Nonetheless, within this data set, there was no significant change observed in the N/P ratio (Figure 3l). Additionally, [Si] displayed an increase of $+0.15 \pm 0.08$ µmol · kg^{-1} · yr^{-1} near $\gamma^n = 27.4$ with no substantial alterations observed in the remaining portions of the water column (Figure 3k).

Across the study period, seawater at 40°S became more acidic due to a change in DIC partially caused by biological processes, calcium carbonate formation and CO_2 uptake. A small decrease of -0.24 ± 0.06 µmol kg^{-1} yr^{-1} in the carbonate pump, C_{carb}, was observed within the first ∼200 m ($\gamma^n < 26.8$ kg m^{-3}) of the water column (Figure 4), correlating closely with the change in A_T (Figure 3c). DIC showed an increase above ∼2,000 m ($\gamma^n \approx 27.9$ kg m^{-3}; Figures 3d and 4) with a maximum $+1.44 \pm 0.11$ µmol kg^{-1} yr^{-1} in the surface waters ($\gamma^n \approx 26.7$ kg m^{-3}; Figures 3d and 4). It is interesting to note that the change in DIC was higher down to 2,000 m

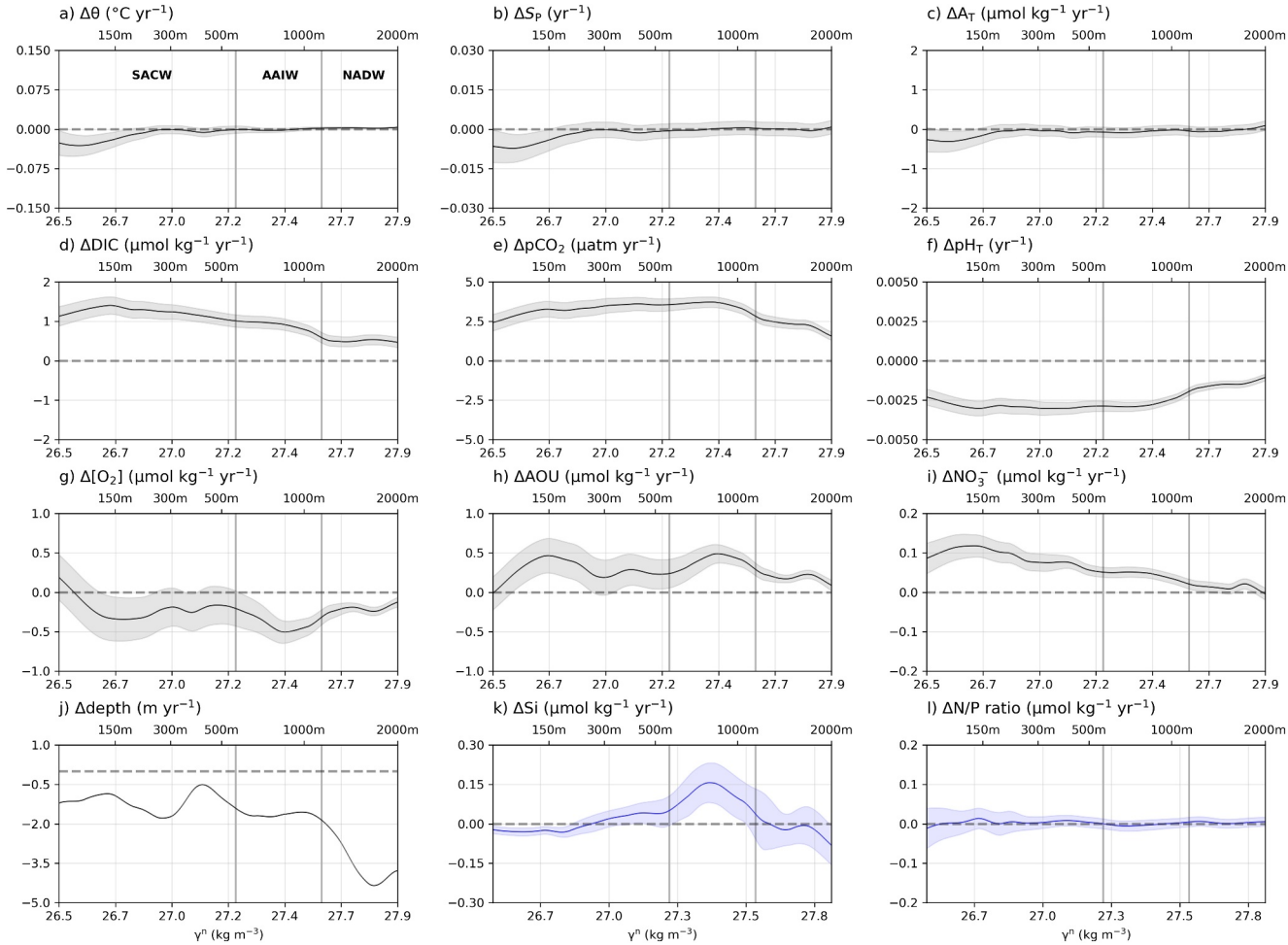

Figure 3. Change in biogeochemical parameters across 40°S in the Atlantic Ocean for all available data. Approximate depths are shown at the top of each plot along water masses as part of subplot a. Note that blue panels k and l only include data up to 2014 as BGC-Argo floats are not equipped for phosphate and silicate measurements. MLD is off the *x*-axis (54m, $\gamma^n \approx 25.8$).

when using all available data, most likely indicative of a deeper penetration depth within the last decade, and noticeable thanks to the high-resolution of BGC-Argo data. Seawater pCO_2 showed a corresponding average increase of $+3.83 \pm 0.15$ μatm yr^{-1}, before slowly converging back to no change deeper than 2000 m ($\gamma^n \approx 27.9$ kg m^{-3}; Figure 3e). These changes were closely followed by an average decrease of -0.002 ± 0.0001 yr^{-1} in pH_T and a maximum decrease of -0.003 ± 0.0001 yr^{-1} in the shallow subsurface (~150 m, $\gamma^n < 26.7$ kg m^{-3}; Figure 3f), where the pH maximum is often located (Arroyo et al., 2022). This change in pH_T is consistent with the most recent globally averaged rate of surface ocean pH change, -0.0016 ± 0.0006 yr^{-1} (Garcia-Soto et al., 2021).

Not all DIC changes were attributed to C_{anth}, as there also appeared to be a significant increase in the soft tissue pump (Figure 4). If calculated using AOU, $C_{soft(AOU)}$ increased by $+0.20 \pm 0.03$ μmol · kg^{-1} · yr^{-1} down to ~2,000 m ($\gamma^n \approx 27.9$ kg m^{-3}; Figure 4), while being close to no change near ~300 m ($\gamma^n \approx 27.0$ kg m^{-3}; Figure 4). The corresponding $C_{anth(AOU)}$ thus represented most of the DIC change, with an increase of $+1.48 \pm 0.13$ μmol · kg^{-1} · yr^{-1} close to the surface ($\gamma^n < 26.7$ kg m^{-3}; Figure 4). However, if calculated using NO_3^-, $C_{soft(NO3)}$ showed an increase ~4 times greater than $C_{soft(AOU)}$, with $+0.85 \pm 0.07$ μmol kg^{-1} yr^{-1} in the surface waters ($\gamma^n < 26.8$ kg m^{-3}; Figure 4), and $C_{anth(NO3)}$ then contributing half of $C_{anth(AOU)}$, with an average increase of $+0.67 \pm 0.14$ μmol kg^{-1} yr^{-1} down to 1,000 m ($\gamma^n \approx 27.5$ kg m^{-3}; Figure 4). The *t*-test revealed that the difference between $C_{soft(NO3)}$ and $C_{soft(AOU)}$ stopped being statistically significant below 500 m ($\gamma^n = 27.15$).

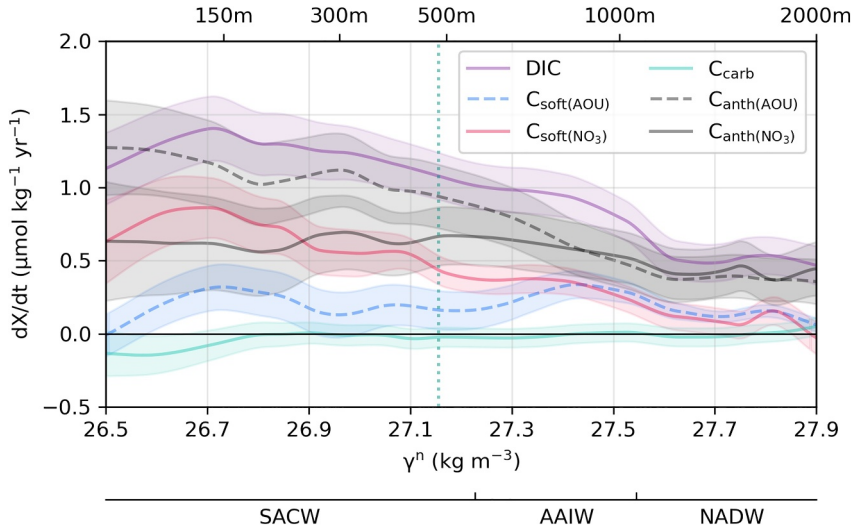

Figure 4. Rates of change in DIC (purple) and its components, C_{carb} (turquoise), $C_{soft(NO3)}$ estimated from NO_3^- (red), $C_{soft(AOU)}$ estimated from AOU (dashed blue), with corresponding $C_{anth(NO3)}$ in solid black and $C_{anth(AOU)}$ in dashed black. Results are for the compilation of all available data. Approximate depths are shown at the top and water masses at the bottom of the axes. MLD is off the *x*-axis (54 m, $\gamma^n \approx 25.8$). The vertical line (dotted green) indicates the neutral density level at which the difference between $C_{soft(NO3)}$ and $C_{soft(AOU)}$ stops being statistically significant (~500 m, $\gamma^n = 27.15$). Separated contributions from both C_{soft} estimates can also be found in Figure S4 in the Supporting Information S1.

Within the study area, the depth-integrated increase in (a) the soft tissue pump was approximately $+0.004 \pm 0.002$ GtC yr^{-1} for $C_{soft(AOU)}$ and $+0.006 \pm 0.002$ GtC yr^{-1} for $C_{soft(NO3)}$, (b) the anthropogenic component was approximately $+0.008 \pm 0.003$ GtC yr^{-1} for $C_{anth(AOU)}$ and $+0.007 \pm 0.003$ GtC yr^{-1} for $C_{anth(NO3)}$ and (c) the carbonate pump C_{carb} was approximately insignificant ($<2 \times 10^{10}$ GtC $yr^{-1} \pm 0.001$ GtC yr^{-1}).

4. Discussion

Although the biological pump at 40°S has clearly strengthened, the magnitude of the increase remains uncertain, depending on whether NO_3^- or AOU is used to estimate the soft tissue pump component. Below, we discuss this uncertainty and the implications of our findings, first looking at the physical factors and subsequently the influence of biology. Attributing the observed BCP changes to different driving factors is beyond the scope of this study, although it deserves further analyses. Here, we discuss how different physical and biogeochemical processes may qualitatively explain our results, as well as the observed discrepancies between the use of NO_3^- and AOU as a proxies for Csoft estimates.

4.1. Influence of Physical Factors on BCP Dynamics

4.1.1. Melting Ice

Variability in oxygen content at 40°S is largely influenced by sea ice dynamics affecting gas exchange, temperature and salinity (Hofmann et al., 2011). The stratification induced by meltwater creates a barrier that inhibits deep water mixing. As a result, vertical water exchange between the surface and deeper ocean layers is slowed, retaining carbon and nutrients in the upper water column for longer, marking a transition from a system that exports carbon and nutrients to one that retains them (Gjelstrup et al., 2022; Priest et al., 2023; von Appen et al., 2021). However, the melting of sea ice cools seawater, enhancing the solubility of CO_2 and O_2 without affecting NO_3^- (Loose et al., 2009). Subsequent air-sea gas exchange will thereby increase DIC and $[O_2]$, but it will not alter AOU because $[O_2]$ changes to match its new saturation level ($[O_2]_{sat}$). Enhanced gas exchange due to stronger surface winds in the South Atlantic, which is a net sink for CO_2, would also increase surface ocean pCO_2 and DIC (Wanninkhof, 2014). This increase in DIC occurs because cooler seawater from melting sea ice can absorb more CO_2 from the atmosphere, assuming that atmospheric CO_2 levels are higher than those in the surface ocean. The impact varies with the supersaturation or undersaturation of surface waters with respect to atmospheric CO_2 and O_2 (Council, 2010; Figuerola et al., 2021). In scenarios of reduced gas exchange due to diminished sea

ice in the Southern Ocean, there should be a decrease in DIC and AOU, as the melting sea ice enhances the ocean's capacity to absorb atmospheric CO_2 and O_2, which would lead the concentrations of these dissolved gases to increase, thus changing $C_{soft(AOU)}$ but not NO_3^- and $C_{soft(NO3)}$. Increased biological productivity, driven by micronutrient influx, releases O_2 into the ocean, potentially leading to local oversaturation; however, this biological O_2 production is often offset by enhanced remineralization at depth, where O_2 is consumed, thereby maintaining overall similar AOU levels.

Melting land ice also enhances ocean stratification and introduces micronutrients such as iron, fueling biological productivity in near-surface waters (Lannuzel et al., 2010, 2016; Morley et al., 2020). Sediment-derived iron, accounting for 54 ± 15% of total iron flux, is carried from continental shelves via benthic diffusion and sediment resuspension (De Jong et al., 2012; Tian et al., 2023). This transport may influence nutrient dynamics and productivity as far as 3,500 km from the Antarctic Peninsula (De Jong et al., 2012). An influx of micronutrients leads to a higher uptake of DIC and also nitrate NO_3^-, resulting in a decrease in $C_{soft(NO3)}$. These changes, predominantly affecting near-surface photosynthesis, align with the Redfield Ratio, which predicts a decrease in NO_3^- proportional to the decrease in DIC. However, this would impact AOU and hence also $C_{soft(AOU)}$ less because O_2 more quickly re-equilibrates with the atmosphere than DIC (Emerson & Hedges, 2008). Enhanced remineralization at greater depths due to the increased productivity would change DIC, AOU, and NO_3^- in line with the Redfield ratio (Henley et al., 2020). As the composition of the water we observe at 40°S is the result of transport of this water from south to north, it also reflects the initial preformed value from the enhanced productivity near the Antarctic as well as processes happening at 40°S and during transport (Morley et al., 2020). Although NO_3^- is generally consumed by biological uptake, localized upwelling or mixing processes can occasionally lead to higher concentrations of NO_3^- in surface waters, reflecting regional variations in nutrient dynamics.

A component of the observed increase in DIC at 40°S could hence reflect both the melting of sea and land ice, which in turn impact the BCP. But unlike for NO_3^-, the AOU change from increased productivity should quickly be masked by air-sea gas exchange, making it impossible to quantify this process using AOU alone. Therefore, the observed changes in AOU at 40°S are not due to melting processes. While changes in NO_3^- could result from these changing endmember conditions, they are influenced by multiple factors such as nutrient dynamics, biological productivity, and vertical water mixing, making NO_3^- an unreliable sole indicator. Consequently, melting ice resulting from global change influences both estimates, although $C_{soft(AOU)}$ may provide a more reliable interpretation. Future research should focus on developing a variable to quantify ice melt in this context, which would enhance our understanding of these processes.

4.1.2. Interior Ocean Mixing

Recent studies have highlighted changes in ocean circulation patterns, which most likely are also reflected at 40°S. Decrease in the ages of Subantarctic Mode Water (SAMW) and Circumpolar Deep Water (CDW) have been observed across the South Atlantic Ocean since the 1990s, suggesting enhanced ventilation, a phenomenon partly attributed to shifts in westerly winds (Fine et al., 2017; Tanhua et al., 2017; Waugh et al., 2013). This trend in SAMW indicates potentially increased isopycnal mixing, which elevates surface DIC due to the upward transport of DIC-rich deep waters, which may drive part of the observed increase in DIC at 40°S (Figure 3d). Additionally, Wei et al. (2022), focusing on a transect from the Rio Grande Rise to the Mid-Atlantic Ridge, demonstrated increases in diapycnal diffusivities, again indicating intensified mixing, thus implying enhanced vertical circulation of nutrient-rich deep waters. This observation is consistent with the observed rise in NO_3^- and $C_{soft(NO3)}$ at 40°S (Figures 3i and 4). Both the isopycnal and diapycnal mixing introduce oxygen-poor deep water to the surface, increasing SACW AOU, especially in regions with high remineralization (Figure 3h; Fine et al., 2017; Tanhua et al., 2017; Waugh et al., 2013). However, AOU does not increase significantly in the top layers of the profile (Figure 3g), which would be expected with the upwelling of deep oxygen-poor waters. This suggests that the apparent increase in remineralization within the BCP as inferred from DIC, AOU, and NO_3^- measurements is primarily due to the enhanced advection of older deep waters to the surface. However, increased winds also drive enhanced upwelling, which similarly elevates DIC, AOU, and NO_3^- in the SACW (Section 4.1.3). Therefore, the observed discrepancy between $C_{soft(NO3)}$ and $C_{soft(AOU)}$ at 40°S cannot be solely attributed to wind-driven upwelling but is also influenced by other processes such as enhanced vertical mixing and advection of older waters.

Piñango et al. (2022) also reported increased organic matter remineralization in the AAIW, likely indicating deoxygenation. This is due to an enhanced flux of organic matter, which increases microbial oxygen consumption, and enhanced ventilation. While the latter introduces oxygen, it also brings in more anthropogenic carbon, exacerbating the oxygen demand for remineralization. The influx of anthropogenic carbon boosts the biological pump's activity, leading to greater production and sinking of organic matter. As this organic matter decomposes, microbial respiration intensifies, consuming more oxygen and further depleting oxygen levels in intermediate waters, thus amplifying the overall deoxygenation effect. This is especially true along the AAIW from 50°S to 30°S, where increased AOU was observed at a mean rate of AOU change of 0.23 ± 0.68 μmol kg^{-1} yr^{-1} south of 30°S, which concurs with our results (Figure 3; Piñango et al., 2022). This is consistent with the deoxygenation trend reported by Santos et al. (2016) for the AAIW in the South Atlantic subtropical gyre from 1960 to 2015, which was -0.18 ± 0.04 μmol kg^{-1} yr^{-1}. It also aligns with the AOU rate observed by Fontela et al. (2021)in the Argentine Basin, which was 0.38 ± 0.13 μmol kg^{-1} yr^{-1}. Additionally, these results agree with the AAIW deoxygenation documented by Schmidtko et al. (2017) over the last two decades.

A component of the observed changes in DIC, AOU, NO_3^- and therefore the BCP at 40°S is thus mechanistically linked to enhanced mixing through an increased influence of deeper waters on overlying water masses.

4.1.3. Wind-Driven Circulation

Increased wind-driven circulation has been invoked to explain changes in marine biogeochemical cycles, including effects on DIC and nutrients (England et al., 2014; Keppler & Landschützer, 2019; Liu et al., 2023).

The rate of gas exchange between the ocean and atmosphere is controlled by a set of physical processes that scale with wind speed (Wanninkhof, 2014). Because the South Atlantic Ocean is a net sink for CO_2 (i.e., seawater pCO_2 is lower than atmospheric pCO_2), enhanced gas exchange due to stronger surface winds would increase surface ocean pCO_2 and DIC. The same process decreases AOU, which is positive in surface waters here (Figure 3h), due to the absorption of atmospheric oxygen. In contrast, dissolved nutrients such as NO_3^- (and therefore $C_{soft(NO3)}$), which are primarily controlled by biological uptake and nutrient cycling, are not directly affected by intensified gas exchange. A component of the observed changes in $C_{soft(NO3)}$ and $C_{soft(AOU)}$ could hence reflect the impact of increased wind-driven circulation. However, the complexity of these interactions makes it impossible to quantify this process using C_{soft} alone. This highlights the need to consider wind-driven effects in conjunction with other drivers, such as enhanced vertical mixing and advection of older waters (Section 4.1.2).

However, as discussed in Section 4.1.2, increased winds drive enhanced upwelling due to intensified wind shear over the surface ocean. Deep waters are enriched in DIC, AOU, and NO_3^- due in a large part to the remineralization of organic matter, so enhanced upwelling elevates all these properties in the SACW roughly in line with the Redfield ratio (Figures 3d, 3h, and 3i; England et al., 2014; Liu et al., 2023). Accordingly, changes in wind-driven circulation would increase both $C_{soft(NO3)}$ and $C_{soft(AOU)}$ in SACW, but likely in agreement with the Redfield ratio and true change in C_{soft}. Therefore, this aspect alone cannot cause the observed discrepancy between $C_{soft(NO3)}$ and $C_{soft(AOU)}$ at 40°S and the influence of interior ocean mixing must hence also be considered (Section 4.1.2).

Additionally, increased mixing due to stronger winds leads to a more uniform distribution of DIC in the upper part of the water column as the surface mixed layer thickens (England et al., 2014), as seen at 40°S (Figure 3j). This mixing increases the AOU near the surface and lowers it at depth. Mixing also results in a more even distribution of nutrients like NO_3^- throughout the water column, redistributing these vertically rather than straightforwardly increasing or decreasing the soft tissue pump. This highlights that the observed changes in DIC, AOU, and NO_3^- are not solely driven by biological processes but are also influenced by physical mixing. It is hence essential to understand the complex interplay of factors affecting these variables. However, unlike NO_3^-, the changes in AOU and DIC are influenced by both physical mixing and air-sea gas exchange, making it impossible to quantify the exact contribution of each process to the observed changes.

4.2. Biological Effects on Quantifying the BCP

Previous sections have highlighted the significant influence of physical processes on the observed changes in DIC, AOU, and NO_3^- at 40°S. Melting ice, both sea and land, affects gas exchange and nutrient dynamics,

leading to changes in DIC and [O_2] without altering NO_3^- directly. Enhanced interior ocean mixing, driven by shifts in ocean circulation, has been shown to elevate surface DIC and NO_3^- due to upward transport of nutrient-rich deep waters. Wind-driven circulation further contributes by increasing gas exchange rates and driving upwelling, which enriches surface waters with DIC, AOU, and NO_3^-.

In addition to physical processes' influence, the increase in NO_3^- at 40°S, especially in the first 500 m (Figure 3i), could reflect increased remineralization, possibly caused by enhanced organic matter export at 40°S (Boyd & Trull, 2007; Sarmiento, 2006). This should be accompanied by an [O_2] decline in the same waters, increasing AOU, which in the surface mixed layer could then be attenuated by oxygen exchange with the atmosphere. Consequently, $C_{soft(AOU)}$ in the near surface would underestimate the actual change in C_{soft}, while in deeper waters beneath the mixed layer (without the associated air-sea gas exchange causing a bias in $C_{soft(AOU)}$), $C_{soft(AOU)}$ would be consistent with $C_{soft(NO3)}$ (Figure 4). However, $C_{soft(AOU)}$ and $C_{soft(NO3)}$ differ significantly from each other down to around 500 m (or 27.15 kg m^{-3}), which is deeper than the mixed layer here (54 m, $\gamma^n \approx 25.8$), so this is not a complete explanation for the discrepancy.

In shallower waters, other factors might explain the observed discrepancy between $\Delta C_{soft(AOU)}$ and $\Delta C_{soft(NO3)}$, such as changes in the stoichiometry of organic matter. Variations from standard plankton biomass elemental ratios (i.e., the Redfield ratio; Redfield, 1958) have been observed spatially and temporally (Inomura et al., 2022; Martiny et al., 2013; Tanioka & Matsumoto, 2020), which may contribute to the difference between $C_{soft(AOU)}$ and $C_{soft(NO3)}$ observed here (Figure 4; Anderson & Sarmiento, 1994). South of 40°S, the carbon to nitrogen (C:N) ratio is closely aligned with the Redfield ratio (Johnson et al., 2022). Conversely, north of 40°S, dissolved organic matter (DOM) has higher C:N ratios, with 10.4 ± 4.1 at 30°S, 14.0 ± 4.8 at 35°S, and 9.7 ± 1.7 at 40°S, all surpassing the Redfield ratio of 6.6 (Johnson et al., 2022). The elevated C:N observed at 40°S could then also result from a changing balance between water masses from the north and the south. Organic matter with higher C:N requires more oxygen for its remineralization, thereby accelerating the consumption of dissolved oxygen (Matsumoto et al., 2020; Szewczyk et al., 2023). Climate change is expected to cause significant stoichiometric shifts in plankton biomass, with warmer temperatures and rising CO_2 levels promoting higher C:P and N:P ratios (Ayo et al., 2017; DeVries, 2018; DeVries et al., 2017; Toseland et al., 2013; van de Waal et al., 2010; Yvon-Durocher et al., 2017) which may result in increased oxygen consumption during remineralization and thus higher AOU (DeVries, 2018). Additionally, variability in the rates of change across the water column could result from changing remineralization depth due to temperature-dependent remineralization (Boscolo-Galazzo et al., 2018, 2021), shifts in particle injection pumps (Boyd et al., 2019), or changes in DOC remineralization with circulation or degradation dynamics (Hansell, 2013).

The enhanced remineralization and possible changes in C:N observed at 40°S may be due to increased diatom populations further south (Arrigo et al., 1999, 2015; Soppa et al., 2016). Diatoms are reliant on silicate and significant nitrate consumers. Also, enhanced inputs of iron are known to stimulate diatom productivity (Section 4.1.1). Diatoms secrete transparent exopolymeric particles (TEP), which act like glue to hold aggregates together, leading to faster sinking of marine particles and a more efficient biological pump (J. Chen & Thornton, 2015; Toullec & Moriceau, 2018). TEP production also increases the C:N ratio (Kim et al., 2021; Passow, 2002). Boosted silicate availability, most likely due to enhanced upwelling and glacial runoff (Henley et al., 2020), may accordingly reduce NO_3^- levels at the sea surface and increase NO_3^- and AOU in the AAIW due to enhanced sinking and remineralization of algal diatom biomass. If driven by diatoms, we would expect the increased NO_3^- and AOU in deeper waters to be accompanied by an increase in [Si] in AAIW (Cael et al., 2021), which is what we observed at 40°S (Figure 3k). Either through remote or via locally enhanced productivity an increased abundance of diatoms, caused by higher iron and [Si], could in part be responsible for the changes in the BCP that we observe.

4.3. Consequences of Changes in the Biological Carbon Pump

4.3.1. Implications for Marine CO_2 Sink

Previous studies have shown that the South Atlantic Ocean is a sink of atmospheric CO_2, with an average net air-to-sea CO_2 flux of 0.3 Pg C yr^{-1} (Takahashi et al., 1997, 2002). Recent work has highlighted strong seasonality in the South Atlantic CO_2 flux, acting as a strong sink during the spring when most primary production takes place, and shifting toward a source during autumn (Lencina-Avila et al., 2016; Padin et al., 2010). Monitoring whether the South Atlantic acts as a source or sink of CO_2 is vital for understanding its role in the global carbon cycle as it

directly influences the atmospheric CO_2 concentration and therefore the Earth's climate (Lencina-Avila et al., 2016; Padin et al., 2010). As these variations are connected to the biological productivity of the South Atlantic Ocean, it is especially important to understand the biological pump's contribution to changes in DIC, which has a direct impact on whether the ocean basin acts as a source or sink of CO_2.

The observed increase in surface ocean pCO_2 at 40°S is consistent with the growth in atmospheric pCO_2 (Figure 3e). If the changes in the BCP were to lead seawater pCO_2 to rise faster or slower than atmospheric pCO_2, this would cause a decrease or increase respectively of the ocean CO_2 sink (DeVries et al., 2017). However, the enhanced BCP that we find suggests that while biological processes are contributing to increased carbon sequestration (Section 4.2), physical processes such as increased mixing may counteract this effect by bringing CO_2-rich waters to the surface (Section 4.1), thereby maintaining the observed consistency with atmospheric pCO_2 growth.

4.3.2. Carbon Export and BCP Role in Climate Responses

Our findings at 40°S indicate that the biological pump is experiencing shifts due to a mix of changes in water mass formation regions and biological factors across the Atlantic Ocean. Model results suggest that the anticipated increase in iron supply and improved light availability for phytoplankton—owing to enhanced near-surface stratification and prolonged ice-free periods—will likely amplify primary production. This could, in turn, boost carbon export around the Antarctic region (Henley et al., 2020). These observations at 40°S may be an early sign of the impact of global change in the Southern Ocean, assuming that our estimates have accounted for the effects of advection and transport on the BCP.

Building on these observations, the depth-integrated increase in organic carbon export flux was between 0.004 ± 0.002 ($C_{soft(AOU)}$) and 0.006 ± 0.002 GtC yr^{-1} ($C_{soft(NO3)}$) for the study area, while the change in the carbonate pump was negligible ($<2 \times 1010$ GtC $yr^{-1} \pm 0.001$ GtC yr^{-1}). For comparison, a recent estimate of global export production accounting for both POC and DOC was 8.37 ± 1.57 GtC yr^{-1} (Sulpis et al., 2023), which amounts to 0.017 ± 0.003 GtC yr^{-1} when scaled down to the study area. This suggests that the increase in the BCP that we observed could represent an increase in the amount of carbon remineralized by 23%–35% each year. However, if the study region is a biological "hotspot" with high baseline productivity and remineralization, the global average would be underestimated for this region, so the 23%–35% increase is an upper bound. The anthropogenic component remained the highest, with $+0.008 \pm 0.003$ GtC yr^{-1} for $C_{anth(AOU)}$ and $+0.007 \pm 0.003$ GtC yr^{-1} for $C_{anth(NO3)}$ which, compared to the global average of 0.005 ± 0.001 for 2022 (2.8 ± 0.4 GtC yr^{-1}; Friedlingstein et al., 2023), implies that the study area also has a higher anthropogenic CO_2 uptake relative to the global average.

It is crucial to note that these estimates assume that changes in export production are fully reflected in changes in remineralization rates at these depths. However, the full variance of these processes throughout the entire water column might not be captured, and changes in remineralization and circulation can also influence C_{soft} independently of direct changes in export production. Thus, while our results show an increase in local export production, it is important to differentiate between export production, carbon remineralization, and sequestration, as these differences in C_{soft} may not correspond directly to changes in export production over these timescales. Additionally, these observations should not be interpreted as being indicative of a consistent global trend, as highlighted by Henson et al. (2022), who found no consistent global increase in export production. While we cannot precisely quantify the influence of each driver on C_{soft} due to the complexity of these interactions, both $C_{soft(AOU)}$ and $C_{soft(NO3)}$ estimates consistently indicate an increase, suggesting an overall intensification of the BCP.

Regardless of its size as a fraction of the baseline remineralization rate, the magnitude of the DIC increase associated with the BCP at 40°S is of the same order of magnitude as the anthropogenic increase in DIC (Figures 3d and 4). Thus, while changes in the biological carbon pump are often considered less significant than anthropogenic CO_2 uptake, they should still be considered in global carbon budgets.

4.3.3. Anthropogenic Influence and CO_2 Dynamics

Since the early 1960s, the primary driver behind the long-term trend in the ocean carbon sink has been the rising uptake of anthropogenic CO_2 (Gruber et al., 2023). From 2004 to 2019, the global oceanic DIC pool increased at

an average rate of 3.2 ± 0.7 Pg C yr^{-1}, with no statistically detectable difference between the total DIC change and C_{anth} accumulation between 2004 and 2020 (Keppler et al., 2023). This implies no global net change in C_{soft} but does not rule out a spatial redistribution driven by various factors including ocean warming, alterations in marine biology, and other physical changes within the oceans, as discussed above for 40°S. Thus, our study may be an example of this redistribution effect—as also witnessed in the northeast Atlantic Ocean (Humphreys et al., 2016). The role of the biological carbon pump relative to anthropogenic CO_2 uptake in changing the marine DIC pool may be more important than previously thought.

However, these findings must be interpreted with caution due to the seasonal biases inherent to the data collection and the variable nature of nutrient concentrations, which challenge the reliability of estimated long-term change estimates. Observations, primarily during the austral summer, may not fully capture the year-round dynamics of the BCP, nutrient fluxes, or the changing properties of water masses, potentially skewing our understanding of the BCP's role in DIC variations and affecting the capacity for C_{anth} uptake by the ocean. Furthermore, Behrenfeld et al. (2006) highlighted the significant impact of climate-driven variability, such as the El Niño-Southern Oscillation, on surface phytoplankton abundance. Thus, this underscores the importance of considering both seasonal and interannual variability.

Finally, although current observations reveal negligible net changes in global C_{soft}, it is essential to acknowledge that model projections indicate potential divergences in these trends on centennial timescales, largely due to the long residence times of C_{soft} (Cao & Zhang, 2017; Siegel et al., 2023). Additionally, the spatial redistribution of C_{soft} may modify nutrient dynamics and alter residence times, which, over extended periods, are likely to result in significant alterations in both C_{soft} and export production (Henson et al., 2022; Wilson et al., 2022).

5. Conclusions

At 40°S in the Atlantic Ocean, from 1972 to 2023, DIC increased, down to approximately 2,000 m ($\gamma^n \approx 27.9$ kg m^{-3}), with a near-surface maximum rate of 1.44 ± 0.11 μmol kg^{-1} yr^{-1}. Although at least half of this change can be attributed to anthropogenic CO_2 accumulation, the intensification of the BCP in this region is evident, with contributions ranging from 0.20 ± 0.03 μmol kg^{-1} yr^{-1} to 0.85 ± 0.07 μmol kg^{-1} yr^{-1} (using $C_{soft(AOU)}$ and $C_{soft(NO3)}$, respectively). While we cannot definitively select one soft tissue pump estimation over another due to inherent uncertainties in the influence of different processes, the concurrent increase in both $C_{soft(AOU)}$ and $C_{soft(NO3)}$ estimates, despite their discrepancies, consistently points toward an intensification of the BCP at this location.

This study at 40°S in the Southern Ocean has also provided valuable insights into the complex interplay of physical, biological, and anthropogenic factors influencing the dynamics of the BCP. Our investigation suggests that no single factor alone accounts for the observed changes in the efficiency of the BCP; rather, it is the cumulative effect of changes in sea ice dynamics, ocean stratification, wind patterns, and biological activity, including photosynthesis and organic matter degradation, which themselves are impacted by ongoing global changes that are not in equilibrium. The precise quantification of each driver's influence and interplay should be the focus of future research.

These findings also highlight the implications of these changes for CO_2 sink behavior and carbon export. The observed increase in pCO_2 at 40°S and the depth-integrated increase in organic carbon export flux imply shifts in the region's role in the global carbon cycle. These shifts are not only vital for understanding the evolution of atmospheric CO_2 concentration but also for potential future climate change mitigation efforts.

Finally, the study addresses the anthropogenic influence on CO_2 dynamics. The increasing uptake of anthropogenic CO_2 and its interplay with the biological carbon pump indicate that the role of the BCP in DIC changes might be more intricate and significant than previously assumed. This highlights the need for comprehensive consideration of the biological carbon pump in global carbon budgets and climate models.

Conflict of Interest

The authors declare no conflicts of interest relevant to this study.

Data Availability Statement

All data and code used in this analysis are available as a GitHub repository (Delaigue, 2024). PyCO2SYS v1.8.1 (Humphreys et al., 2022) was used to solve for the carbonate system (Humphreys et al., 2024). The Gibbs-SeaWater (GSW) Oceanographic Toolbox was used to calculate neutral density (McDougall & Barker, 2011). Figures were made with Python version 3.9 (van Rossum & Drake Jr, 2009).

Acknowledgments

We would like to express our sincere gratitude to the Global Ocean Data Analysis Project (GLODAP) for providing invaluable oceanographic data, which significantly enhanced the quality and depth of our research. The comprehensive data set offered by GLODAP played a pivotal role in this study. We also extend our appreciation to the BGC-Argo program for the deployment of biogeochemical Argo floats. The data collected by BGC-Argo floats were instrumental in updating our data set with recent trends. Finally, we would like to acknowledge our colleagues and research team for their dedication and hard work throughout this project. This paper would not have been possible without the collective contributions of these individuals and organizations. Any errors or omissions remain our own. LD also wishes to thank the Institut de la mer de Villefranche (France) and in particular the OMTAB team for hosting her during the later stage of this research project. This research was supported by the Netherlands Organization for Scientific Research (NWO-VENI Grant VI.Veni.212.086 to O.S).

References

Anderson, L. A., & Sarmiento, J. L. (1994). Redfield ratios of remineralization determined by nutrient data analysis. *Global Biogeochemical Cycles*, *8*(1), 65–80. https://doi.org/10.1029/93gb03318

Arrigo, K. R., Robinson, D. H., Worthen, D. L., Dunbar, R. B., DiTullio, G. R., Van Woert, M., & Lizotte, M. P. (1999). Phytoplankton community structure and the drawdown of nutrients and CO_2 in the Southern Ocean. *Science*, *283*(5400), 365–367. https://doi.org/10.1126/science.283.5400.365

Arrigo, K. R., van Dijken, G. L., & Strong, A. L. (2015). Environmental controls of marine productivity hot spots around Antarctica. *Journal of Geophysical Research: Oceans*, *120*(8), 5545–5565. https://doi.org/10.1002/2015JC010888

Arroyo, M. C., Fassbender, A. J., Carter, B. R., Edwards, C. A., Fiechter, J., Norgaard, A., & Feely, R. A. (2022). Dissimilar sensitivities of ocean acidification metrics to anthropogenic carbon accumulation in the Central North Pacific Ocean and California current large marine ecosystem. *Geophysical Research Letters*, *49*(15), e2022GL097835. https://doi.org/10.1029/2022GL097835

Ayo, B., Abad, N., Artolozaga, I., Azua, I., Baña, Z., Unanue, M., et al. (2017). Imbalanced nutrient recycling in a warmer ocean driven by differential response of extracellular enzymatic activities. *Global Change Biology*, *23*(10), 4084–4093. https://doi.org/10.1111/gcb.13779

Behrenfeld, M. J., O'Malley, R. T., Siegel, D. A., McClain, C. R., Sarmiento, J. L., Feldman, G. C., et al. (2006). Climate-driven trends in contemporary ocean productivity. *Nature*, *444*(7120), 752–755. https://doi.org/10.1038/nature05317

Bittig, H. C., Maurer, T. L., Plant, J. N., Schmechtig, C., Wong, A. P. S., Claustre, H., et al. (2019). A BGC-Argo Guide: Planning, deployment, data handling and usage. *Frontiers in Marine Science*, *6*. [Review]. https://doi.org/10.3389/fmars.2019.00502

Boscolo-Galazzo, F., Crichton, K. A., Barker, S., & Pearson, P. N. (2018). Temperature dependency of metabolic rates in the upper ocean: A positive feedback to global climate change? *Global and Planetary Change*, *170*, 201–212. https://doi.org/10.1016/j.gloplacha.2018.08.017

Boscolo-Galazzo, F., Crichton, K. A., Ridgwell, A., Mawbey, E. M., Wade, B. S., & Pearson, P. N. (2021). Temperature controls carbon cycling and biological evolution in the ocean twilight zone. *Science*, *371*(6534), 1148–1152. https://doi.org/10.1126/science.abb6643

Boyd, P. W., Claustre, H., Levy, M., Siegel, D. A., & Weber, T. (2019). Multi-faceted particle pumps drive carbon sequestration in the ocean. *Nature*, *568*(7752), 327–335. https://doi.org/10.1038/s41586-019-1098-2

Boyd, P. W., & Trull, T. W. (2007). Understanding the export of biogenic particles in oceanic waters: Is there consensus? *Progress in Oceanography*, *72*(4), 276–312. https://doi.org/10.1016/j.pocean.2006.10.007

Browning, T. J., Bouman, H. A., Moore, C. M., Schlosser, C., Tarran, G. A., Woodward, E. M. S., & Henderson, G. M. (2014). Nutrient regimes control phytoplankton ecophysiology in the South Atlantic. *Biogeosciences*, *11*(2), 463–479. https://doi.org/10.5194/bg-11-463-2014

Buesseler, K. O., Antia, A. N., Chen, M., Fowler, S. W., Gardner, W. D., Gustafsson, O., et al. (2007). An assessment of the use of sediment traps for estimating upper ocean particle fluxes. *Journal of Marine Research*, *65*(3), 345–416. https://doi.org/10.1357/002224007781567621

Cael, B. B., Dutkiewicz, S., & Henson, S. (2021). Abrupt shifts in 21st-century plankton communities. *Science Advances*, *7*(44), eabf8593. https://doi.org/10.1126/sciadv.abf8593

Cao, L., & Zhang, H. (2017). The role of biological rates in the simulated warming effect on oceanic CO_2 uptake. *Journal of Geophysical Research: Biogeosciences*, *122*(5), 1098–1106. https://doi.org/10.1002/2016JG003756

Chen, C.-T. A. (1978). Decomposition of calcium carbonate and organic carbon in the deep oceans. *Science*, *201*(4357), 735–736. https://doi.org/10.1126/science.201.4357.735

Chen, J., & Thornton, D. C. (2015). Transparent exopolymer particle production and aggregation by a marine planktonic diatom (Thalassiosira weissflogii) at different growth rates. *Journal of Phycology*, *51*(2), 381–393. https://doi.org/10.1111/jpy.12285

Council, N. R. (2010). *Ocean acidification: A national strategy to meet the challenges of a changing ocean*. The National Academies Press. https://doi.org/10.17226/12904

Davila, X., Gebbie, G., Brakstad, A., Lauvset, S. K., McDonagh, E. L., Schwinger, J., & Olsen, A. (2022). How is the ocean anthropogenic carbon reservoir filled? *Global Biogeochemical Cycles*, *36*(5), e2021GB007055. https://doi.org/10.1029/2021GB007055

De Jong, J., Schoemann, V., Lannuzel, D., Croot, P., de Baar, H., & Tison, J. L. (2012). Natural iron fertilization of the Atlantic sector of the Southern Ocean by continental shelf sources of the Antarctic Peninsula. *Journal of Geophysical Research*, *117*(G1), G01029. https://doi.org/10.1029/2011jg001679

Delaigue, L. (2024). louisedelaigue/SA-BCP-change: v1.2 (v1.2) [Software]. *Zenodo*. https://doi.org/10.5281/zenodo.12735206

De La Rocha, C. L., & Passow, U. (2014). 8.4—The biological pump. In H. D. Holland & K. K. Turekian (Eds.), *Treatise on Geochemistry* (2nd ed., pp. 93–122). Elsevier. https://doi.org/10.1016/B978-0-08-095975-7.00604-5

DeVries, T. (2018). New directions for ocean nutrients. *Nature Geoscience*, *11*(1), 15–16. https://doi.org/10.1038/s41561-017-0042-z

DeVries, T., Holzer, M., & Primeau, F. (2017). Recent increase in oceanic carbon uptake driven by weaker upper-ocean overturning. *Nature*, *542*(7640), 215–218. https://doi.org/10.1038/nature21068

Dickson, A. G. (1990). Standard potential of the reaction: $AgCl(s) + 12H_2(g) = Ag(s) + HCl(aq)$, and and the standard acidity constant of the ion HSO_4^- in synthetic sea water from 273.15 to 318.15 K. *The Journal of Chemical Thermodynamics*, *22*(2), 113–127. https://doi.org/10.1016/0021-9614(90)90074-Z

Dickson, A. G. (1992). The determination of total dissolved inorganic carbon in sea water using extraction/coulometry: The first stage of a collaborative study. https://www.osti.gov/biblio/5823722

Dickson, A. G., & Riley, J. P. (1979). The estimation of acid dissociation constants in sea-water media from potentiometric titrations with strong base. II. The dissociation of phosphoric acid. *Marine Chemistry*, *7*(2), 101–109. https://doi.org/10.1016/0304-4203(79)90002-1

Emerson, S., & Hedges, J. (2008). *Chemical oceanography and the marine carbon cycle*. Cambridge University Press.

England, M. H., McGregor, S., Spence, P., Meehl, G. A., Timmermann, A., Cai, W., et al. (2014). Recent intensification of wind-driven circulation in the Pacific and the ongoing warming hiatus. *Nature Climate Change*, *4*(3), 222–227. https://doi.org/10.1038/nclimate2106

Feely, R. A., Sabine, C. L., Lee, K., Berelson, W., Kleypas, J., Fabry, V. J., & Millero, F. J. (2004). Impact of anthropogenic CO_2 on the CaCO3 system in the oceans. *Science*, *305*(5682), 362–366. https://doi.org/10.1126/science.1097329

Figuerola, B., Hancock, A. M., Bax, N., Cummings, V. J., Downey, R., Griffiths, H. J., et al. (2021). A Review and meta-analysis of potential impacts of ocean acidification on marine calcifiers from the southern ocean. *Frontiers in Marine Science*, *8*. [Review]. https://doi.org/10.3389/fmars.2021.584445

Fine, R. A., Peacock, S., Maltrud, M. E., & Bryan, F. O. (2017). A new look at ocean ventilation time scales and their uncertainties. *Journal of Geophysical Research: Oceans*, *122*(5), 3771–3798. https://doi.org/10.1002/2016JC012529

Fontela, M., Velo, A., Gilcoto, M., & Pérez, F. F. (2021). Anthropogenic CO_2 and ocean acidification in Argentine Basin Water Masses over almost five decades of observations. *Science of the Total Environment*, *779*, 146570. https://doi.org/10.1016/j.scitotenv.2021.146570

Friedlingstein, P., O'Sullivan, M., Jones, M. W., Andrew, R. M., Bakker, D. C. E., Hauck, J., et al. (2023). Global carbon budget 2023. *Earth System Science Data*, *15*(12), 5301–5369. https://doi.org/10.5194/essd-15-5301-2023

Fritsch, F. N., & Carlson, R. E. (1980). Monotone Piecewise cubic interpolation. *SIAM Journal on Numerical Analysis*, *17*(2), 238–246. https://doi.org/10.1137/0717021

Garcia, H. E., & Gordon, L. I. (1992). Oxygen solubility in seawater: Better fitting equations. *Limnology & Oceanography*, *37*(6), 1307–1312. https://doi.org/10.4319/lo.1992.37.6.1307

Garcia-Soto, C., Cheng, L., Caesar, L., Schmidtko, S., Jewett, E. B., Cheripka, A., et al. (2021). An Overview of ocean climate change indicators: Sea surface temperature, ocean heat content, ocean pH, dissolved oxygen concentration, Arctic sea ice extent, thickness and volume, sea level and strength of the AMOC (Atlantic meridional overturning circulation). *Frontiers in Marine Science*, *8*. [Review]. https://doi.org/10.3389/fmars.2021.642372

Gjelstrup, C. V. B., Sejr, M. K., de Steur, L., Christiansen, J. S., Granskog, M. A., Koch, B. P., et al. (2022). Vertical redistribution of principle water masses on the Northeast Greenland Shelf. *Nature Communications*, *13*(1), 7660. https://doi.org/10.1038/s41467-022-35413-z

Groeskamp, S., Lenton, A., Matear, R., Sloyan, B. M., & Langlais, C. (2016). Anthropogenic carbon in the ocean—Surface to interior connections. *Global Biogeochemical Cycles*, *30*(11), 1682–1698. https://doi.org/10.1002/2016GB005476

Gruber, N., Bakker, D. C. E., DeVries, T., Gregor, L., Hauck, J., Landschützer, P., et al. (2023). Trends and variability in the ocean carbon sink. *Nature Reviews Earth and Environment*, *4*(2), 119–134. https://doi.org/10.1038/s43017-022-00381-x

Gruber, N., Clement, D., Carter, B. R., Feely, R. A., van Heuven, S., Hoppema, M., et al. (2019). The oceanic sink for anthropogenic CO_2 from 1994 to 2007. *Science*, *363*(6432), 1193–1199. https://doi.org/10.1126/science.aau5153

Gruber, N., Sarmiento, J., Robinson, A., McCarthy, J., & Rothschild, B. (2002). *The Sea: Ideas and observations on progress in the study of the seas*. Wiley.

Gruber, N., Sarmiento, J. L., & Stocker, T. F. (1996). An improved method for detecting anthropogenic CO_2 in the oceans. *Global Biogeochemical Cycles*, *10*(4), 809–837. https://doi.org/10.1029/96gb01608

Hansell, D. A. (2013). Recalcitrant dissolved organic carbon fractions. *Annual Review of Marine Science*, *5*(1), 421–445. https://doi.org/10.1146/annurev-marine-120710-100757

Heinze, C., Maier-Reimer, E., & Winn, K. (1991). Glacial pCO_2 reduction by the world ocean: Experiments with the Hamburg carbon cycle model. *Paleoceanography*, *6*(4), 395–430. https://doi.org/10.1029/91PA00489

Henley, S. F., Cavan, E. L., Fawcett, S. E., Kerr, R., Monteiro, T., Sherrell, R. M., et al. (2020). Changing biogeochemistry of the southern ocean and its ecosystem implications. *Frontiers in Marine Science*, *7*. [Original Research]. https://doi.org/10.3389/fmars.2020.00581

Henson, S. A., Laufkötter, C., Leung, S., Giering, S. L. C., Palevsky, H. I., & Cavan, E. L. (2022). Uncertain response of ocean biological carbon export in a changing world. *Nature Geoscience*, *15*(4), 248–254. https://doi.org/10.1038/s41561-022-00927-0

Henson, S. A., Sanders, R., & Madsen, E. (2012). Global patterns in efficiency of particulate organic carbon export and transfer to the deep ocean. *Global Biogeochemical Cycles*, *26*(1). https://doi.org/10.1029/2011gb004099

Hofmann, A. F., Peltzer, E. T., Walz, P. M., & Brewer, P. G. (2011). Hypoxia by degrees: Establishing definitions for a changing ocean. *Deep Sea Research Part I: Oceanographic Research Papers*, *58*(12), 1212–1226. https://doi.org/10.1016/j.dsr.2011.09.004

Humphreys, M. P., Griffiths, A. M., Achterberg, E. P., Holliday, N. P., Rérolle, V. M., Menzel Barraqueta, J. L., et al. (2016). Multidecadal accumulation of anthropogenic and remineralized dissolved inorganic carbon along the Extended Ellett Line in the northeast Atlantic Ocean. *Global Biogeochemical Cycles*, *30*(2), 293–310. https://doi.org/10.1002/2015gb005246

Humphreys, M. P., Lewis, E. R., Sharp, J. D., & Pierrot, D. (2022). PyCO2SYS v1.8: Marine carbonate system calculations in Python. *Geoscientific Model Development*, *15*(1), 15–43. https://doi.org/10.5194/gmd-15-15-2022

Humphreys, M. P., Schiller, A. J., Sandborn, D., Gregor, L., Pierrot, D., van Heuven, S. M. A. C., et al. (2024). PyCO2SYS: Marine carbonate system calculations in Python (v1.8.3.2). *Zenodo*. https://doi.org/10.5281/zenodo.12564139

Inomura, K., Deutsch, C., Jahn, O., Dutkiewicz, S., & Follows, M. J. (2022). Global patterns in marine organic matter stoichiometry driven by phytoplankton ecophysiology. *Nature Geoscience*, *15*(12), 1034–1040. https://doi.org/10.1038/s41561-022-01066-2

Ito, T., & Follows, M. J. (2005). Preformed phosphate, soft tissue pump and atmospheric CO_2. *Journal of Marine Research*, *63*(4), 813–839. https://doi.org/10.1357/0022240054663231

Johnson, K. S., Mazloff, M. R., Bif, M. B., Takeshita, Y., Jannasch, H. W., Maurer, T. L., et al. (2022). Carbon to nitrogen uptake ratios observed across the southern ocean by the SOCCOM profiling float array. *Journal of Geophysical Research: Oceans*, *127*(9), e2022JC018859. https://doi.org/10.1029/2022JC018859

Jones, D. C., Ito, T., Takano, Y., & Hsu, W.-C. (2014). Spatial and seasonal variability of the air-sea equilibration timescale of carbon dioxide. *Global Biogeochemical Cycles*, *28*(11), 1163–1178. https://doi.org/10.1002/2014GB004813

Keppler, L., & Landschützer, P. (2019). Regional wind variability modulates the southern ocean carbon sink. *Scientific Reports*, *9*(1), 7384. https://doi.org/10.1038/s41598-019-43826-y

Keppler, L., Landschützer, P., Lauvset, S. K., & Gruber, N. (2023). Recent trends and variability in the oceanic storage of dissolved inorganic carbon. *Global Biogeochemical Cycles*, *37*(5), e2022GB007677. https://doi.org/10.1029/2022GB007677

Khatiwala, S., Primeau, F., & Hall, T. (2009). Reconstruction of the history of anthropogenic CO_2 concentrations in the ocean. *Nature*, *462*(7271), 346–349. https://doi.org/10.1038/nature08526

Khatiwala, S., Tanhua, T., Mikaloff Fletcher, S., Gerber, M., Doney, S. C., Graven, H. D., et al. (2013). Global ocean storage of anthropogenic carbon. *Biogeosciences*, *10*(4), 2169–2191. https://doi.org/10.5194/bg-10-2169-2013

Kim, H.-J., Kim, H. J., Yang, E.-J., Cho, K.-H., Jung, J., Kang, S.-H., et al. (2021). Temporal and spatial variations in particle fluxes on the Chukchi Sea and East Siberian Sea Slopes from 2017 to 2018. *Frontiers in Marine Science*, *7*. [Original Research]. https://doi.org/10.3389/fmars.2020.609748

Landschützer, P., Gruber, N., Haumann, F. A., Rödenbeck, C., Bakker, D. C. E., van Heuven, S., et al. (2015). The reinvigoration of the Southern Ocean carbon sink. *Science*, *349*(6253), 1221–1224. https://doi.org/10.1126/science.aab2620

Lannuzel, D., Schoemann, V., De Jong, J., Pasquer, B., Van der Merwe, P., Masson, F., et al. (2010). Distribution of dissolved iron in Antarctic sea ice: Spatial, seasonal, and inter-annual variability. *Journal of Geophysical Research*, *115*(G3), G03022. https://doi.org/10.1029/2009jg001031

Lannuzel, D., Vancoppenolle, M., Van der Merwe, P., De Jong, J., Meiners, K. M., Grotti, M., et al. (2016). Iron in sea ice: Review and new insights. *Elementa: Science of the Anthropocene*, *4*. https://doi.org/10.12952/journal.elementa.000130
Laufkötter, C., Vogt, M., Gruber, N., Aumont, O., Bopp, L., Doney, S. C., et al. (2016). Projected decreases in future marine export production: The role of the carbon flux through the upper ocean ecosystem. *Biogeosciences*, *13*(13), 4023–4047. https://doi.org/10.5194/bg-13-4023-2016
Lauvset, S. K., Lange, N., Tanhua, T., Bittig, H. C., Olsen, A., Kozyr, A., et al. (2022). GLODAPv2. 2022: The latest version of the global interior ocean biogeochemical data product. *Earth System Science Data*, *14*(12), 5543–5572. https://doi.org/10.5194/essd-14-5543-2022
Lee, K., Tong, L. T., Millero, F. J., Sabine, C. L., Dickson, A. G., Goyet, C., et al. (2006). Global relationships of total alkalinity with salinity and temperature in surface waters of the world's oceans. *Geophysical Research Letters*, *33*(19), L19605. https://doi.org/10.1029/2006gl027207
Lencina-Avila, J. M., Ito, R. G., Garcia, C. A. E., & Tavano, V. M. (2016). Sea-air carbon dioxide fluxes along 35°S in the South Atlantic Ocean. *Deep Sea Research Part I: Oceanographic Research Papers*, *115*, 175–187. https://doi.org/10.1016/j.dsr.2016.06.004
Li, G., Cheng, L., Zhu, J., Trenberth, K. E., Mann, M. E., & Abraham, J. P. (2020). Increasing ocean stratification over the past half-century. *Nature Climate Change*, *10*(12), 1116–1123. https://doi.org/10.1038/s41558-020-00918-2
Liu, Y., Moore, J. K., Primeau, F., & Wang, W. L. (2023). Reduced CO_2 uptake and growing nutrient sequestration from slowing overturning circulation. *Nature Climate Change*, *13*(1), 83–90. https://doi.org/10.1038/s41558-022-01555-7
Loose, B., Schlosser, P., Smethie, W., & Jacobs, S. (2009). An optimized estimate of glacial melt from the Ross Ice Shelf using noble gases, stable isotopes, and CFC transient tracers. *Journal of Geophysical Research*, *114*(C8), C08007. https://doi.org/10.1029/2008jc005048
Marsay, C. M., Sanders, R. J., Henson, S. A., Pabortsava, K., Achterberg, E. P., & Lampitt, R. S. (2015). Attenuation of sinking particulate organic carbon flux through the mesopelagic ocean. *Proceedings of the National Academy of Sciences of the United States of America*, *112*(4), 1089–1094. https://doi.org/10.1073/pnas.1415311112
Martiny, A. C., Pham, C. T. A., Primeau, F. W., Vrugt, J. A., Moore, J. K., Levin, S. A., & Lomas, M. W. (2013). Strong latitudinal patterns in the elemental ratios of marine plankton and organic matter. *Nature Geoscience*, *6*(4), 279–283. https://doi.org/10.1038/ngeo1757
Matsumoto, K., Tanioka, T., & Rickaby, R. (2020). Linkages between dynamic phytoplankton C: N: P and the ocean carbon cycle under climate change. *Oceanography*, *33*(2). https://doi.org/10.5670/oceanog.2020.203
McDougall, T. J., & Barker, P. M. (2011). *Getting started with TEOS-10 and the Gibbs Seawater (GSW) oceanographic toolbox* (Vol. 127, pp. 1–28). SCOR/IAPSO WG.
Mignot, A., D'Ortenzio, F., Taillandier, V., Cossarini, G., & Salon, S. (2019). Quantifying observational errors in biogeochemical-argo oxygen, nitrate, and chlorophyll a concentrations. *Geophysical Research Letters*, *46*(8), 4330–4337. https://doi.org/10.1029/2018GL080541
Moore, J. K., Doney, S. C., Glover, D. M., & Fung, I. Y. (2001). Iron cycling and nutrient-limitation patterns in surface waters of the World Ocean. *Deep Sea Research Part II: Topical Studies in Oceanography*, *49*(1), 463–507. https://doi.org/10.1016/S0967-0645(01)00109-6
Morley, S. A., Abele, D., Barnes, D. K. A., Cárdenas, C. A., Cotté, C., Gutt, J., et al. (2020). Global drivers on southern ocean ecosystems: Changing physical environments and anthropogenic pressures in an Earth system. *Frontiers in Marine Science*, *7*. [Review]. https://doi.org/10.3389/fmars.2020.547188
Nowicki, M., DeVries, T., & Siegel, D. A. (2024). The influence of air-sea CO_2 disequilibrium on carbon sequestration by the oceanocean's biological pump. *Global Biogeochemical Cycles*, *38*(2), e2023GB007880. https://doi.org/10.1029/2023GB007880
Orr, J. C., Fabry, V. J., Aumont, O., Bopp, L., Doney, S. C., Feely, R. A., et al. (2005). Anthropogenic ocean acidification over the twenty-first century and its impact on calcifying organisms. *Nature*, *437*(7059), 681–686. https://doi.org/10.1038/nature04095
Padin, X., Vázquez-Rodríguez, M., Castaño, M., Velo, A., Alonso-Pérez, F., Gago, J., et al. (2010). Air-sea CO_2 fluxes in the Atlantic as measured during boreal spring and autumn. *Biogeosciences*, *7*(5), 1587–1606. https://doi.org/10.5194/bg-7-1587-2010
Parekh, P., Dutkiewicz, S., Follows, M. J., & Ito, T. (2006). Atmospheric carbon dioxide in a less dusty world. *Geophysical Research Letters*, *33*(3), L03610. https://doi.org/10.1029/2005GL025098
Passow, U. (2002). Transparent exopolymer particles (TEP) in aquatic environments. *Progress in Oceanography*, *55*(3), 287–333. https://doi.org/10.1016/S0079-6611(02)00138-6
Piñango, A., Kerr, R., Orselli, I. B. M., Carvalho, A. d. C. O., Azar, E., Karstensen, J., & Garcia, C. A. E. (2022). Ocean acidification and long-term changes in the carbonate system properties of the South Atlantic Ocean. *Global Biogeochemical Cycles*, *36*(9), e2021GB007196. https://doi.org/10.1029/2021GB007196
Polovina, J. J., Howell, E. A., & Abecassis, M. (2008). Ocean's least productive waters are expanding. *Geophysical Research Letters*, *35*(3), L03618. https://doi.org/10.1029/2007GL031745
Priest, T., von Appen, W.-J., Oldenburg, E., Popa, O., Torres-Valdés, S., Bienhold, C., et al. (2023). Atlantic water influx and sea-ice cover drive taxonomic and functional shifts in Arctic marine bacterial communities. *The ISME Journal*, *17*(10), 1612–1625. https://doi.org/10.1038/s41396-023-01461-6
Redfield, A. C. (1958). The biological control of chemical factors in the environment. *American Scientist*, *46*(3), 230A-221.
Redfield, A. C. (1963). The influence of organisms on the composition of seawater. *Sea*, *2*, 26–77. Retrieved from https://ci.nii.ac.jp/naid/10003517839/en/
Riebesell, U., Körtzinger, A., & Oschlies, A. (2009). Sensitivities of marine carbon fluxes to ocean change. *Proceedings of the National Academy of Sciences of the United States of America*, *106*(49), 20602–20609. https://doi.org/10.1073/pnas.0813291106
Sabine, C. L., Feely, R. A., Gruber, N., Key, R. M., Lee, K., Bullister, J. L., et al. (2004). The oceanic sink for anthropogenic CO_2. *Science*, *305*(5682), 367–371. https://doi.org/10.1126/science.1097403
Sabine, C. L., & Tanhua, T. (2010). Estimation of anthropogenic CO_2 inventories in the ocean. *Annual Review of Marine Science*, *2*(1), 175–198. https://doi.org/10.1146/annurev-marine-120308-080947
Santos, G. C., Kerr, R., Azevedo, J. L. L., Mendes, C. R. B., & da Cunha, L. C. (2016). Influence of Antarctic intermediate water on the deoxygenation of the Atlantic Ocean. *Dynamics of Atmospheres and Oceans*, *76*, 72–82. https://doi.org/10.1016/j.dynatmoce.2016.09.002
Sarmiento, J. L. (2006). *Ocean biogeochemical dynamics*. Princeton university press.
Sarmiento, J. L., Hughes, T. M. C., Stouffer, R. J., & Manabe, S. (1998). Simulated response of the ocean carbon cycle to anthropogenic climate warming. *Nature*, *393*(6682), 245–249. https://doi.org/10.1038/30455
Sarmiento, J. L., Orr, J. C., & Siegenthaler, U. (1992). A perturbation simulation of CO_2 uptake in an ocean general circulation model. *Journal of Geophysical Research*, *97*(C3), 3621–3645. https://doi.org/10.1029/91JC02849
Sauzède, R., Claustre, H., Uitz, J., Jamet, C., Dall'Olmo, G., D'Ortenzio, F., et al. (2016). A neural network-based method for merging ocean color and Argo data to extend surface bio-optical properties to depth: Retrieval of the particulate backscattering coefficient. *Journal of Geophysical Research: Oceans*, *121*(4), 2552–2571. https://doi.org/10.1002/2015JC011408
Schlunegger, S., Rodgers, K. B., Sarmiento, J. L., Frölicher, T. L., Dunne, J. P., Ishii, M., & Slater, R. (2019). Emergence of anthropogenic signals in the ocean carbon cycle. *Nature Climate Change*, *9*(9), 719–725. https://doi.org/10.1038/s41558-019-0553-2

Schmidtko, S., Stramma, L., & Visbeck, M. (2017). Decline in global oceanic oxygen content during the past five decades. *Nature*, *542*(7641), 335–339. https://doi.org/10.1038/nature21399

Siegel, D. A., DeVries, T., Cetinić, I., & Bisson, K. M. (2023). Quantifying the oceanocean's biological pump and its carbon cycle impacts on global scales. *Annual Review of Marine Science*, *15*(1), 329–356. https://doi.org/10.1146/annurev-marine-040722-115226

Soppa, M. A., Völker, C., & Bracher, A. (2016). Diatom phenology in the southern ocean: Mean patterns, trends and the role of climate oscillations. *Remote Sensing*, *8*(5), 420. https://doi.org/10.3390/rs8050420

Sulpis, O., Lauvset, S. K., & Hagens, M. (2020). Current estimates of K1* and K2* appear inconsistent with measured CO_2 system parameters in cold oceanic regions. *Ocean Science*, *16*(4), 847–862. https://doi.org/10.5194/os-16-847-2020

Sulpis, O., Trossman, D. S., Holzer, M., Jeansson, E., Lauvset, S. K., & Middelburg, J. J. (2023). Respiration patterns in the dark ocean. *Global Biogeochemical Cycles*, *37*(8), e2023GB007747. https://doi.org/10.1029/2023GB007747

Szewczyk, C. J., Smith, E. M., & Benitez-Nelson, C. R. (2023). Temperature sensitivity of oxygen demand varies as a function of organic matter source. *Frontiers in Marine Science*, *10*. [Original Research]. https://doi.org/10.3389/fmars.2023.1133336

Tagliabue, A., Sallée, J.-B., Bowie, A. R., Lévy, M., Swart, S., & Boyd, P. W. (2014). Surface-water iron supplies in the Southern Ocean sustained by deep winter mixing. *Nature Geoscience*, *7*(4), 314–320. https://doi.org/10.1038/ngeo2101

Takahashi, T., Feely, R. A., Weiss, R. F., Wanninkhof, R. H., Chipman, D. W., Sutherland, S. C., & Takahashi, T. T. (1997). Global air-sea flux of CO_2: An estimate based on measurements of sea–air pCO_2 difference. *Proceedings of the National Academy of Sciences of the United States of America*, *94*(16), 8292–8299. https://doi.org/10.1073/pnas.94.16.8292

Takahashi, T., Sutherland, S. C., Sweeney, C., Poisson, A., Metzl, N., Tilbrook, B., et al. (2002). Global sea–air CO_2 flux based on climatological surface ocean pCO_2, and seasonal biological and temperature effects. *Deep Sea Research Part II: Topical Studies in Oceanography*, *49*(9–10), 1601–1622. https://doi.org/10.1016/S0967-0645(02)00003-6

Tanhua, T., Hoppema, M., Jones, E. M., Stöven, T., Hauck, J., Dávila, M. G., et al. (2017). Temporal changes in ventilation and the carbonate system in the Atlantic sector of the Southern Ocean. *Deep Sea Research Part II: Topical Studies in Oceanography*, *138*, 26–38. https://doi.org/10.1016/j.dsr2.2016.10.004

Tanioka, T., & Matsumoto, K. (2020). A meta-analysis on environmental drivers of marine phytoplankton C: N: P. *Biogeosciences*, *17*(11), 2939–2954. https://doi.org/10.5194/bg-17-2939-2020

Tian, H.-A., van Manen, M., Bunnell, Z. B., Jung, J., Lee, S. H., Kim, T.-W., et al. (2023). Biogeochemistry of iron in coastal Antarctica: Isotopic insights for external sources and biological uptake in the Amundsen sea polynyas. *Geochimica et Cosmochimica Acta*, *363*, 51–67. https://doi.org/10.1016/j.gca.2023.10.029

Toggweiler, J., Gnanadesikan, A., Carson, S., Murnane, R., & Sarmiento, J. L. (2003). Representation of the carbon cycle in box models and GCMs: 1. Solubility pump. *Global Biogeochemical Cycles*, *17*(1). https://doi.org/10.1029/2001gb001401

Toseland, A., Daines, S. J., Clark, J. R., Kirkham, A., Strauss, J., Uhlig, C., et al. (2013). The impact of temperature on marine phytoplankton resource allocation and metabolism. *Nature Climate Change*, *3*(11), 979–984. https://doi.org/10.1038/nclimate1989

Toullec, J., & Moriceau, B. (2018). Transparent exopolymeric particles (TEP) selectively increase biogenic Silica dissolution from Fossil diatoms as compared to Fresh diatoms. *Frontiers in Marine Science*, *5*. [Original Research]. https://doi.org/10.3389/fmars.2018.00102

Uppström, L. R. (1974). The boron/chlorinity ratio of deep-sea water from the Pacific Ocean. *Deep-Sea Research and Oceanographic Abstracts*, *21*(2), 161–162. https://doi.org/10.1016/0011-7471(74)90074-6

van de Waal, D. B., Verschoor, A. M., Verspagen, J. M., van Donk, E., & Huisman, J. (2010). Climate-driven changes in the ecological stoichiometry of aquatic ecosystems. *Frontiers in Ecology and the Environment*, *8*(3), 145–152. https://doi.org/10.1890/080178

Van Rossum, G., & Drake, F. L. (2009). *Python reference manual* (Vol. 111, pp. 1–52). Centrum voor Wiskunde en Informatica.

Virtanen, P., Gommers, R., Oliphant, T. E., Haberland, M., Reddy, T., Cournapeau, D., et al. (2020). SciPy 1.0: Fundamental algorithms for scientific computing in Python. *Nature Methods*, *17*(3), 261–272. https://doi.org/10.1038/s41592-019-0686-2

Volk, T., & Hoffert, M. I. (1985). Ocean carbon pumps: Analysis of relative strengths and efficiencies in ocean-driven atmospheric CO_2 changes. In *The carbon cycle and atmospheric CO_2: Natural variations Archean to present* (pp. 99–110). https://doi.org/10.1029/GM032p0099

von Appen, W.-J., Waite, A. M., Bergmann, M., Bienhold, C., Boebel, O., Bracher, A., et al. (2021). Sea-ice derived meltwater stratification slows the biological carbon pump: Results from continuous observations. *Nature Communications*, *12*(1), 7309. https://doi.org/10.1038/s41467-021-26943-z

Wanninkhof, R. (2014). Relationship between wind speed and gas exchange over the ocean revisited. *Limnology and Oceanography: Methods*, *12*(6), 351–362. https://doi.org/10.4319/lom.2014.12.351

Waugh, D. W., Primeau, F., DeVries, T., & Holzer, M. (2013). Recent changes in the ventilation of the southern oceans. *Science*, *339*(6119), 568–570. https://doi.org/10.1126/science.1225411

Wei, J., Gunn, K. L., & Reece, R. (2022). Mid-ocean ridge and storm enhanced mixing in the central South Atlantic Thermocline. *Frontiers in Marine Science*, *8*. [Original Research]. https://doi.org/10.3389/fmars.2021.771973

Williams, N. L., Juranek, L. W., Feely, R. A., Johnson, K. S., Sarmiento, J. L., Talley, L. D., et al. (2017). Calculating surface ocean pCO_2 from biogeochemical Argo floats equipped with pH: An uncertainty analysis. *Global Biogeochemical Cycles*, *31*(3), 591–604. https://doi.org/10.1002/2016GB005541

Williams, R. G., & Follows, M. J. (2011). *Ocean dynamics and the carbon cycle: Principles and mechanisms*. Cambridge University Press. https://doi.org/10.1017/CBO9780511977817

Wilson, J. D., Andrews, O., Katavouta, A., de Melo Viríssimo, F., Death, R. M., Adloff, M., et al. (2022). The biological carbon pump in CMIP6 models: 21st century trends and uncertainties. *Proceedings of the National Academy of Sciences of the United States of America*, *119*(29), e2204369119. https://doi.org/10.1073/pnas.2204369119

Wolf-Gladrow, D. A., Zeebe, R. E., Klaas, C., Körtzinger, A., & Dickson, A. G. (2007). Total alkalinity: The explicit conservative expression and its application to biogeochemical processes. *Marine Chemistry*, *106*(1–2), 287–300. https://doi.org/10.1016/j.marchem.2007.01.006

Yvon-Durocher, G., Schaum, C.-E., & Trimmer, M. (2017). The temperature dependence of phytoplankton stoichiometry: Investigating the roles of species sorting and local Adaptation. *Frontiers in Microbiology*, *8*. [Original Research]. https://doi.org/10.3389/fmicb.2017.02003